Development of Direct Born–Oppenheimer Molecular Dynamics with Applications to Water Clusters and Mechanochemistry

Vladimir V. Rybkin

Series of dissertations submitted to the
Faculty of Mathematics and Natural Sciences, University of Oslo
No. 1572

ISSN 1501-7710

Cover: Hanne Baadsgaard Utigard.
Printed in Norway: AIT Oslo AS.

Produced in co-operation with Akademika Publishing.
The thesis is produced by Akademika Publishing merely in connection with the thesis defence. Kindly direct all inquiries regarding the thesis to the copyright holder or the unit which grants the doctorate.

Contents

Acknowledgements

I am using this opportunity to express my appreciation to everyone, who made the successful completion of my PhD possible. Foremost, I would like to express my gratitude to my supervisors Prof. Trygve Helgaker and Prof. Einar Uggerud for their expertise, guidance and for giving me the opportunity to work with them at the University of Oslo. I would also like to acknowledge the collaborators in my research: Dr. Ulf Ekström, Dr. Simen Reine, Dr. Vebjørn Bakken, Dr. Hans Sverre Smaløand Anton Simakov at the University of Oslo; Prof. Wim Klopper at Karlsruhe Institute of Technology; Dr. Thomas Kjærgaard at Aarhus University. Without their contributions, none of my research projects would be fulfilled.

I would like to express a special gratitude to the Centre for Theoretical and Computational Chemistry (CTCC), mentioning with pleasure some of its current and former members: Kai Kaarvann Lange, Dr. Erik Tellgren, Johannes Rekkedal, Patrick Merlot, Alexey Zatula, Jon Austad, Ass. Prof. Thomas Bondo Perersen, Dr. Anrew Teale and Dr. Michal Przybytek. Every single talk with them contributed to my professional growth, general knowledge and personal maturing. I must confess that none of my articles was scheduled in the PhD plan. They were rather a result of fruitful scientific cross-fertilization flourishing within the CTCC. Besides providing an excellent scientific and social environment, the CTCC generously funded my participation in the European School in Quantum Chemistry (2009), Sostrup Summer School - Quantum Chemistry and Molecular Properties (2010) as well as in many conferences in Norway and abroad. For me, it was an honour to be a part of the CTCC, Oslo.

I am grateful for the Quota scheme of the Norwegian government for the financial support of my PhD research and again to CTCC for improving my living standard beyond the standard Quota scholarship. I would like to express my gratitude to Prof. Svein Samdal and the CTCC managers - John McNicol, Anne Marie Øveraas and Jan Ingar Johnsen - for helping a stranger to adapt in Norway. I thank Prof. Poul Jørgensen for orginizing my short but productive visit to Aarhus University.

Besides, I would like to acknowledge Dr. Andrey Yachmenev (University College of London) for proof reading Chapter 1 and discussing fundamental theoretical questions as well as to Dr. Yury Minenkov (King Abdullah University of Science and Technology) and Dr. Konstantinos Vogiatzis (University of Minnesota) for useful discussions.

Finally, I would like to thank my parents - Marina and Vladimir - for giving birth to me and bringing me up, my sister Elena and niece Lada for believing in my success and especialy to my wife Tatiana for loving support and infinite patience during my nordic scientific Odyssey.

Preface

This thesis have been prepared under the supervision of prof. T. Helgaker and prof. E. Uggerud during my PhD studies at the University of Oslo in 2008-2012 as well as during my subsequent stays at the Karlsruhe Institute of Technology and G.A. Krestov Institute of Solution Chemistry of the Russian Academy of Sciences (Ivanovo) the last two years. Most of the work have been done on method and code development, although applications constitute a very significant share. The main theoretical method to be developed as well as the main tool for the applications was Born-Oppenheimer molecular dynamics. Most code development has been done in Dalton program suite.

Exploration of potential energy surfaces, even mostly by Born-Oppenheimer molecular dynamics, is a very vast area of theoretical chemistry. Thus, it is impossible to embrace everything. Moreover, as there are many worlds in the Everett's interpretation of quantum mechanics, there exist many worlds, known as schools or traditions, in theoretical chemistry: molecular quantum chemistry, condensed-phase plane-wave school, theoretical spectroscopy, force-field world ... They deal with similar problems (including potential energy surfaces) but not necessarily overlap. For instance, notations and terminology are not seldom quite different. Density functional theory calculations may be called *ab initio* (first principles) or not. Molecular dynamics is sometimes defined with explicit reference to empirical force fields ignoring its *ab initio* counterpart and so on.

Bearing the generality of the topic and the manifold of approaches to it in mind, I tried to make my account of general theory rather personalized than complete. Of course, this does not mean that the derivations and logic of narration have been developed exclusively by me. Quite on the contrary: most (but not all!) are borrowed. Still, the selection of what to put in the thesis reflects my views of the field. Regarding myself as a member of the "molecular quantum chemistry" school, I, nevertheless, tried to take "the best of the many-worlds" avoiding confusions in notation and terminology. However, some eclecticism is inevitably present.

The thesis contains seven chapters. Chapters 1-5 are devoted to theoretical issues: the Born-Oppenheimer approximation, electronic structure theory, potential energy surfaces exploration, coordinate systems and transformations, and Born-Oppenheimer molecular dynamics. My own theoretical contributions are referenced in Chapters 4 (the HOPE back-transformation) and 5 (sampling trajectories in internal coordinates) and are smoothly built into the narration. By obvious reasons, they are paid more attention to than they would be in a non-biased account. Unlike my theoretical work, the code development issues and applications are discussed in separate chapters, Chapter 6 and 7, respectively. The applications – dynamics of the water clusters and the mechanochemistry of alkanes – are quite different from one another but united by the common theoretical and computational approach.

... well, in fact he had not done such great things in science. I believe indeed he had done nothing at all. But that's very often the case, of course, with men of science among us in Russia.

Fyodor Dostoevsky, The Devils
(Translated from the Russian by
Constance Garnett)

Chapter 1

Born-Oppenheimer approximation

Let us consider a molecule consisting of N nuclei and $l-N$ electrons. The Schrödinger equation for this system in the Cartesian coordinate frame that has the origin at nuclei center of mass is then written as follows [1]:

$$\hat{H}_{\mathrm{rve}}\Psi^m(\mathbf{R},\mathbf{r}) = E^m\Psi^m(\mathbf{R},\mathbf{r}). \tag{1.1}$$

Here, **R** and **r** are coordinates of the nuclei and the electrons respectively, $\hat{H}_{\mathrm{rve}}$ is the rovibronic Hamiltonian, $\Psi^m(\mathbf{R},\mathbf{r})$ is the rovibronic wave function corresponding to quantum state m and E^m is the corresponding energy. The rovibronic Hamiltonian is:

$$\hat{H}_{\mathrm{rve}} = \hat{T}_{\mathrm{e}}^0 + \hat{T}_{\mathrm{e}}' + \hat{T}_{\mathrm{N}} + V(\mathbf{R},\mathbf{r}). \tag{1.2}$$

In this equation:

$$\hat{T}_{\mathrm{e}}^0 = -\frac{\hbar^2}{2m_{\mathrm{e}}}\sum_{i=N+1}^{l}\nabla_i^2, \tag{1.3}$$

$$\hat{T}_{\mathrm{e}}' = -\frac{\hbar^2}{2M_{\mathrm{N}}}\sum_{i,j=N+1}^{l}\nabla_i\nabla_j, \tag{1.4}$$

$$\hat{T}_{\mathrm{N}} = -\frac{\hbar^2}{2}\sum_{i=2}^{N}\frac{\nabla_i^2}{m_i} + \frac{\hbar^2}{2M_{\mathrm{N}}}\sum_{i,j=2}^{N}\nabla_i\nabla_j, \tag{1.5}$$

$$V(\mathbf{R},\mathbf{r}) = \sum_{r<s=l}^{l}\frac{Z_rZ_se^2}{4\pi\epsilon_0R_{rs}}, \tag{1.6}$$

where m_i is the mass of the ith nucleus, M_{N} is the total mass of all the nuclei, m_{e} is the mass of the electron, Z_re is the charge of each particle (in atomic units, it is equal to -1 for an electron and to the atomic number Z_r for nuclei), and R_{rs} is the separation between sth and rth particles.

One can introduce the electronic Hamiltonian as

$$\hat{H}_{\mathrm{e}} = \hat{T}_{\mathrm{e}} + V(\mathbf{r},\mathbf{R}), \tag{1.7}$$

and solve the Schrödinger equation for the electronic wave functions $\Phi^n(\mathbf{r},\{\mathbf{R}\})$ (of electronic

state n):

$$\hat{H}_{\mathrm{e}}\Phi^n(\mathbf{r},\{\mathbf{R}\}) = E_{\mathrm{e}}^n\Phi^n(\mathbf{r},\{\mathbf{R}\}). \tag{1.8}$$

Electronic wave functions $\Phi^n(\mathbf{r},\{\mathbf{R}\})$ depend on the coordinates of the electrons $\mathbf{r}$ explicitly and parametrically on the coordinates of the nuclei $\mathbf{R}$. Having obtained the complete set of electronic wave functions by solving equation (1.8) one can expand the rovibronic wave function as follows:

$$\Psi^m(\mathbf{R},\mathbf{r}) = \sum_{n'} \chi_m^{n'}(\mathbf{R})\Phi^{n'}(\mathbf{r},\{\mathbf{R}\}), \tag{1.9}$$

where functions $\chi_m^{n'}(\mathbf{R})$ depending only on $\mathbf{R}$ serve as coefficients and are to be determined. The summation must be done over both bound and nonbound electronic states. Otherwise, the set formed by the corresponding wave functions is not complete. Ansantz (1.9) is known as the Born-Huang expansion [2]. Substituting it into the Scrödinger equation (1.1), multiplying on the left by Φ^{n*} and integrating over the coordinates of the electrons, one obtains a set of equations for $\chi_m^n(\mathbf{R})$:

$$[\hat{T}_{\mathrm{N}} + E_{\mathrm{e}}^n(\mathbf{R}) - E^m]\chi_m^n(\mathbf{R}) + \sum_{n'} C_{nn'}\chi_m^{n'}(\mathbf{R}) = 0, \tag{1.10}$$

where

$$C_{nn'} = \langle\Phi^n|\hat{T}_{\mathrm{e}}' + \hat{T}_{\mathrm{N}}|\Phi^{n'}\rangle. \tag{1.11}$$

These equations are in principle exact and the approximations are introduced depending on how the coefficients $C_{nn'}$ are treated. If all of them are neglected then the expression for the rovibronic wave function is reduced to a simple product:

$$\Psi^m(\mathbf{R},\mathbf{r}) = \Phi^n(\mathbf{r},\{\mathbf{R}\})\chi_m^n(\mathbf{R}), \tag{1.12}$$

where $\Phi^n(\mathbf{R})$ is the solution of the electronic equation (1.8) and $\chi_m^n(\mathbf{R})$ is the solution of the nuclear Schrödinger equation:

$$[\hat{T}_{\mathrm{N}} + E_{\mathrm{e}}^n(\mathbf{R})]\chi_m^n(\mathbf{R}) = E_n^m\chi_m^n(\mathbf{R}). \tag{1.13}$$

If only the diagonal coefficients C_{nn} are taken into account, then one obtains the adiabatic approximation, in which the rovibronic wave function is still a product (5.4). However, in the nuclear equation (1.13), the Hamiltonian is modified by adding $\langle\Phi^n|\hat{T}_{\mathrm{e}}' + \hat{T}_{\mathrm{N}}|\Phi^n\rangle$ known as adiabatic correction. Higher approximations are known as non-adiabatic.

Mathematically, Born-Oppenheimer and adiabatic approximations are the separation of variables: nuclear and electronic coordinates. Such separation significantly simplifies the solution of the molecular Scrödinger equation (1.1) splitting it into two steps: first, the electronic equation (1.8) is to be solved, then the nuclear one (1.13) for a selected electronic state. A closer inspection of the latter shows that the total electronic energy $E_e^n(\{\mathbf{R}\})$ serves as the potential energy for the nuclei. Since electronic wave function depends on $\mathbf{R}$ parametrically, there is a different electronic Hamiltonian (and set of energy eigenvalues, respectively) for each geometric configuration of the nuclei. Thus, to solve the nuclear equation exactly, one needs to compute $E_e^n(\{\mathbf{R}\})$ for the whole range of $\mathbf{R}$. Since the electronic energy serves as the potential

for the nuclei, hereafter we shall denote it as $V(\mathbf{R})$ and call it the *potential energy surface* (PES). PES is a sum of the electronic energy (including nuclear-electron attraction) and the nuclear-nuclear repulsion. The former can be shown to be continuous everywhere. When the latter is added, discontinuities appear when the nuclei coincide in space. Therefore, PES is a smooth function of $\mathbf{R}$ almost everywhere and has the dimensionality $3N-3$ if the centre of mass is separated and no other approximations introduced. If the rotation of the molecule as a whole is separated then PES dimensionality is reduced to $3N-6$ (or $3N-5$ for a linear molecule) which is usually the case. For each electronic state n, there is a PES defining a set of nuclear wave functions $\chi_m^n(\mathbf{R})$, referred to as rovibrational states. The PES concept is valid for both the Born-Oppenheimer and adiabatic approximations. However, for the former $V(\mathbf{R})$ does not depend on the nuclear masses, which is not the case for the latter since the adiabatic correction depends on m_i. In some approximations based on the effective Hamiltonians the nuclear masses are made geometry-dependent to absorb some of the non-adiabatic effects [3].

Physical rationale beyond the Born-Oppenheimer separation lies in the dramatic differences in the masses of nuclei and electrons. Since the kinetic energy operator for the nuclei $\hat{T}_N$ has the former in the denominator, the $C_{nn'}$ are usually small, that is the motion of the nuclei is too slow to affect the motion of the electrons [4]. Therefore, the Born-Oppenheimer approximation is also known as the "frozen nuclei" approximation. The same logic applies to the adiabatic correction which is usually small as well. It can be shown that the Born-Oppenheimer approximation holds if the energy separation between electronic states is at least two orders greater than the separation between rovibrational states [5].

The Born-Oppenheimer approximation not only lays down a practical way of solving the Schrödinger equation for molecular systems, but also gives birth to the concepts constituting the significant share of the modern chemical terminology [6]. Such concepts as electronic structure of matter, nuclear dynamics, electronic, vibrational and rotational spectra and so on all stem from the Born-Oppenheimer approximation. Even most non-adiabatic approaches use the Born-Oppenheimer concepts such as PES and employ electronic structure calculations.

Historically, the Born-Oppenheimer approximation was used in the pioneering articles on quantum chemistry, although implicitly [7]. In the work of Heitler and London on the hydrogen molecule [8], believed to be the first quantum-chemical article, several potential energy curves for H_2 were reported without the discussion of the separation of the degrees of freedom of electrons and nuclei. This was in 1927, several months before the article of Born and Oppenheimer [5] came out, where mathematical justification for what had already been intuitively grasped was provided. In fact, initial approach of Born and Oppenheimer is based on perturbation theory and is very different from variational derivation of Born and Huang used here. Nevertheless, the results obtained by both approaches are similar.

Chapter 2

Electronic structure theory

Exact solution of the electronic Scrödinger equation for systems containing more than one electron cannot be obtained. Brute-force numerical solutions of it are prohibitively expensive. Therefore, a number of approximations and approximation hierarchies have been introduced to obtain electronic wave functions Φ. All approximate wave functions are supposed to exhibit some important properties of the exact wave function in order to be physically justified. We begin our consideration with these requirements (within non-relativistic framework) [9]:

- Φ must be an eigenfunction of the number operator, the eigenvalue being the number of electrons;
- Φ must obey to the Pauli principle, that is be antisymmetric with respect to permutation of coordinates of any pair of electrons;
- Wave function must be square-integrable;
- Φ must be variational since variational principle is equivalent to the Schtödinger equation [4];
- Exact wave function is size-extensive: for a system consisting of non-interacting subsystems Φ is multiplicative and the energy is additive with respect to fragment wave functions and energies respectfully;
- Hamiltonian eigenstates must be also eigenfunctions of total and projected spin operators;
- Exact wave functions are subject to electronic and nuclear cusp conditions, that is Φ becomes singular when two electrons coincide in space or an electron coincides with a nucleus;
- At large distances electron density corresponding to Φ decays exponentially with distance;
- All properties calculated from the wave function must be invariant under gauge transformations of the potentials of any external fields applied to the system.

Many electronic structure methods originate from the Hartree-Fock-Roothaan (or simply Hartree-Fock, HF) method both conceptually and computationally. The HF method assumes

that the wave function is constructed as antisymmetrized product of one-electron functions known as *spin-orbitals* [4]. Spin-orbitals depend on three spatial and one spin coordinate of the electron. Expressed in a closed form, this type of wave function is known as a *Slater determinant*. Antisymmetrization is imposed by the Pauli principle. Representing Φ as a product of one-electron functions is analogous to finding the probability of independent events. That is why the HF method is also known as the independent particle approximation.

Orbitals, which are spin-orbitals integrated over the spin coordinate, can be expressed as linear combinations of some basis functions. The common way is to use atom-centered functions, originally atomic orbitals, for this purpose. This variant of the HF method is known as "molecular orbitals as linear combinations of atomic orbitals" (MO LCAO), or the Roothaan-Hall method. Currently, other function types are used as basis functions. The energy is variationally optimized with respect to the MO LCAO coefficients, which are varied until the energy converges. Therefore, the *self-consistent field* method is one more name for the HF approximation. Since MO LCAO is the standard technique for the HF approach in quantum chemistry, hereafter we refer to it also as the HF method.

The HF method is a variational and size-extensive method, some variants of which preserve correct spin-symmetry. By construction, the HF wave function obeys Pauli principle and is an eigen function of the number operator. It turns out that the HF method generally covers about 99% of electronic energy and thus embraces most physical effects of molecular systems [9]. However, for accurate calculations this is not enough. The effects beyond the HF approximation are attributed to *electron correlation*. Nevertheless, the HF method still is a milestone of quantum chemistry since it lays down the way to further improvements. It can be shown that Slater determinants form a complete basis in the space of antisymmetric N-electron square-integrable functions. Thus, by expanding Φ as a linear combination of them (N-electron expansion) one is able to build a more accurate approximation. Another way of improving the accuracy for both HF and post-HF calculations is to improve the orbitals, used to construct Slater determinants, that is to improve the one-electron expansion.

2.1 Ab initio methods

Ab initio, or *first principles*, methods are based on systematic employment of N-electron expansion. Indeed, Slater determinants (or electronic configurations) form a basis in the N-electron space. Therefore, Φ obtained variationally as a linear combination of them is the exact solution of the Schrödinger equation in a given one-electron basis (for a given set of orbitals). This method is called *full configuration interaction* (FCI). Orbitals can be obtained by solving HF equations, or else any set of orthonormal orbitals can be used. Slater determinants are constructed by applying excitation operators to the HF determinant, known as the reference determinant. Excitation removes an electron (or several electrons) from the occupied orbital and places it to a virtual one. Mathematically, this is replacing one or some of the spin-orbitals in a Slater determinant with other spin-orbitals.

In practice, FCI wave functions are computationally so expensive that they can only be obtained for very small systems. Therefore, numerous ways of truncating the N-electron expansion, or the CI expansion, and finding the coefficients have been developed. The most obvious

and conceptually simple method is to restrict the number of configurations and optimize the coefficients variationally. This family of methods is called *configuration interaction*. By including only singly and doubly excited determinants one gets CISD wave function, by including triple excitations - CISDT - and so on until the FCI limit is met. Truncated CI methods are variational, but lack size-extensivity. Moreover, the CI expansion converges to the FCI limit very slowly. Therefore, these methods are seldom used now.

A more elaborate approach is the *coupled-cluster* (CC) method. In this approach, the size-extensivity problem of the truncated CI wave functions is solved by using the exponential ansatz for constructing N-electron expansion, rather then the linear one. Along with size-extensivity, at the same level of excitation and with compatible computational effort, the CC methods provide more accurate results than the CI methods. Although standard CC approach is not variational, CC wave functions in practice exhibit some properties implicit to variational approach, most importantly, appending the N-electron expansion lowers the energy. These properties have made the CC methods the most successful in *ab initio* quantum chemistry.

An alternative approach is based on the Rayleigh-Schrödinger perturbation theory and is called *many-body perturbation theory* (MBPT), or *Møller-Plesset* perturbation theory (MPPT). In these methods, the perturbation operator is the difference between the true Coulomb potential of the electron-electron interaction and the effective one of the HF method. By applying the standard perturbation theory techniques, it can be shown that in this framework, the sum of the occupied orbitals energies is the zero order approximation to the energy, whereas the HF energy is the first-order correction. Thus, electron correlation is included starting from the second order in perturbation. The MPPT methods are size-extensive by construction, but often they exhibit non-uniform convergence of the series, for instance, third-order corrected energy can be higher than the second-order corrected. Moreover, this expansion does not have to converge at all. This circumstance restricts the usage of the MPPT methods. Still, the second-order MPPT (MP2) is a popular method accessible for quite large systems. In fact, it is the simplest and the fastest correlated *ab initio* method.

All these techniques, especially the CC theory, have been proven to be able to give accurate description of the variety of molecular properties provided that electronic states are well separated from one another. In the presence of degenerate or near-degenerate states, they are not that successful. In particular, this situation is common for chemical reactions, which assume breaking of one and formation of other bonds. This problem can be fixed by applying excitations not to a single reference determinant, but to several of them, that is to employ a *multi-reference* approach in contrast to a single-reference one, discussed above. While the starting point for the latter is a HF wave function, for the former the reference wave function is obtained by *multi-configurational self-consistent field* (MCSCF) method. In this approach, both the MO LCAO and the CI coefficients are variationally optimized simultaneously. Conceptually, the same machinery can be applied to the MCSCF wave function as to the HF one, giving birth to the *multi-reference* (MR) CI, CC and PT approximations. MR methods are computationally very expensive, but able to describe chemical reactions quite accurately. These techniques should be applied for describing transition states and performing accurate reaction dynamics calculations. The most established and widely used techniques are MRCI and variations of MRPT, while the MRCC methods are still in the process of making.

On top of both single- and multi-reference methods, one can apply *explicitly correlated*

techniques, which are designed to satisfy the electronic cusp condition by introducing the distance between the electrons into the wave function explicitly [10]. This approach is extremely accurate, but computationally demanding and currently restricted to very small molecules.

In general, *ab initio* methods constitute several hierarchies (CC, CI, MPPT, MR-CI ...), within each the approximations are systematically improvable by appending the N-electron expansion. Thus, it its possible to obtain very accurate solutions of the electronic Schrödinger equation. However, the price for this is a very high cost of calculations, which restricts the usage of *ab initio* methods to small and medium-sized molecular systems.

2.2 Density functional theory

Density functional theory (DFT) is an approach alternative to *ab initio* methods. DFT is conceptually based on the Hohenberg-Kohn theorem [11], which states that for electronic ground state, all properties are uniquely determined by the electron density ρ. ρ depends only on three spatial coordinates and, being integrated over space, gives the number of electrons N in the system. Hohenberg and Kohn have also shown that there exists the energy functional of ρ – a density functional – which is minimized by the exact ground state density by the procedure known as the Hohenberg-Kohn variational principle. Although this principle has laid down the conceptual basis for DFT, it lacks some important mathematical properties. These problems have been fixed by Lieb, whose variational principle [12] is used for constructing and minimizing density functionals. Potentially, DFT can reduce a 3N-dimensional problem of finding Ψ to a 3-dimensional problem of finding ρ. However, the form of the exact density functional is not known and, in practice, various approximations have to be introduced.

Most practical DFT methods are based on the Kohn-Sham (KS) theory which treats electrons as non-interacting particles moving in some external potential [13]. The density of such a system can be the same as for the system of interacting electrons, if the potential is chosen properly. This independent-particle approach yields the SCF-like formalism. Technically, the corresponding KS equations are solved similarly to the HF equations: by varying the MO LCAO coefficients until the self-consistency has been achieved. The difference is in the effective one-electron Hamiltonian: in case of HF, it is the Fock operator, whereas in the KS theory it is the KS potential plus the kinetic operator (identical to the one in the Fock operator).

The KS potential includes the external potential (for molecules it is the Coulomb potential generated by the nuclei), and the electron-electron interactions. The latter are expressed as a sum of Coulomb and exchange-correlation, V_{XC} terms. V_{XC} is the functional of electron density. Since its form is not known, it is the point where most DFT approximations are introduced [14]. The simplest one is the *local density approximation* (LDA). In LDA, V_{XC} depends only on the density at the position, where it is calculated, that is LSA is exact for ideal electron gas. *Local spin density approximation* (LSDA) is a generalization of LDA, which takes the Pauli principle into account. A step forward has been made by introducing *generalized-gradient approximations* [14, 15]. In GGA methods, V_{XC} depends not only on the density but also on its gradient at the point, where the potential is evaluated. If some part of the exchange energy is calculated from the HF theory (the so called exact exchange), the functional is called *hybrid*. GGA and the hybrid approaches provide only the guidelines for constructing the functionals,

so that the working formulae for V_{XC} are obtained *ad hoc*. Frequently, empirical parameters are used for that purpose.

We also note that although DFT is a ground-state theory, it is possible to access excited states by the *time-dependent* DFT [17]. Thus, one important restriction is theoretically removed, broadening the range of possible DFT applications.

The *ad hoc* character of the DFT approximations reflects the performance of the method: it may vary from almost quantitatively accurate to not even qualitatively correct [14]. However, generally GGA and especially hybrid functionals perform quite well for ground-state properties around the PES minima for molecules without low-lying excited electronic states. They poorly describe reaction barriers and intermolecular interactions, which restricts the use of DFT for dynamics simulations. In addition, DFT methods do not form any hierarchy, so that there is no possibility for systematic improvement of the description. Still, DFT is the only practically applicable family of methods for overwhelming number of chemically interesting systems due to the low computational cost. Therefore, benchmarking of the functionals is a very important branch of modern computational chemistry [18, 19].

2.3 One-electron expansion and molecular integrals evaluation

The problems of one-electron basis functions choice and the evaluation of molecular integrals are connected in an obvious way. A Slater determinant is an antisymmetrized product of molecular orbitals, which are in turn linear combinations of basis functions. Therefore, calculating any observable quantity one finally faces the integrals of the type $\int \chi_1\chi_2...\chi_n\hat{O}\chi_1\chi_2...\chi_n d\mathbf{r}_1 d\mathbf{r}_2...d\mathbf{r}_n$, where χ_i are real-valued basis functions and $\hat{O}$ is the operator corresponding to the observable. Therefore, the basis functions are not only supposed to describe the orbitals in an accurate and compact way, but also allow for accurate and fast evaluation of molecular integrals. This procedure always consumes a significant share of the computational time. For SCF-type calculations this is the dominant share [9].

Basis sets of Gaussian functions, or simply *Gaussian basis sets*, are a compromise between the quality of the orbitals description and the convenience of the integrals evaluation. A primitive Cartesian Gaussian function has the following form:

$$G_{ijk}(\mathbf{r}, a, \mathbf{A}) = x_A^i y_A^j z_A^z exp(-ar_{\mathrm{A}}^2), \tag{2.1}$$

where $\mathbf{A}(x_A, y_A, z_A)$ is the position of the nucleus, $\mathbf{r}$ is the position of the electron, and r_A is the distance between the latter and the former. The sum of i, j and k gives the total angular momentum quantum number l. Gaussian functions are smooth at $\mathbf{A}$ and, consequently, are poorly suited to describe the nuclear cusp. Furthermore, atomic orbitals decay exponentially rather than as $exp(-ar^2)$. Despite that drawbacks, Gaussians are generally rather similar to atomic orbitals, for example, they have the similar node structure. Gaussian functions are separable in Cartesian directions. Moreover, the Gaussian product rule states that a product of two Gaussians is still a Gaussian function. Due to these two features, the evaluation of molecular integrals is much simplified. In fact, Coulomb interactions can be calculated in a simple man-

ner with Gaussians analytically. Many efficient methods – both analytic and numerical – for evaluation of molecular integrals over Gaussian basis functions have been developed by now [20].

These special properties make Gaussian basis sets the standard choice for one-electron expansions, at least for molecular calculations. Obtaining a reasonable Gaussian basis set is often difficult. It employs optimization of exponents a and possibly contraction coefficients (if a fixed linear combination is supposed to serve as one function) in atomic calculations. In molecular calculations, they are not varied anymore. For the HF and the correlated calculations, the basis set requirements are quite different and the same applies to different properties. As a consequence, there are no standard sets equally fit for various types of calculations. Still, there exist flexible and compact basis sets for most common purposes [9].

There is a price one has to pay for using basis sets justified rather chemically and computationally, than mathematically. Indeed, employment of atom-centered basis functions, including Gaussians, reflect the well known fact that the formation of chemical bonds involves only the outer shells of atoms, leaving the inner ones almost intact. Consequently, even small sets of atom-centered Gaussians are sufficient to capture the essence of chemical bonding and to reconstruct the general picture. Despite this, Gaussian basis sets obviously do not form a basis in one-electron space as they lack completeness. In addition, the usage of atom-centered basis functions leads to the dependence of wave function on the nuclei positions. This gives rise to several complications. First of all, the conditions for the Hellman-Feynman theorem are not satisfied, so that in can not be applied anymore [21]. Secondly, incompleteness gives rise to the *basis set superposition error* [22]. To overcome these difficulties, several alternative approaches employing complete basis sets (e.g. wavelets [23, 24] or using multi-resolution analysis [25, 26]) are being developed, but they are currently unavailable for the routine use.

2.4 Geometric derivatives of energy

For the exploration of PES, it is vital to be able to compute not only the electronic energy but also its derivatives with respect to nuclear coordinates (see Chapter 3). In this chapter, we will use E rather than V for electronic energy as it is more common in electronic structure theory. In the ideal case, the derivatives can be calculated according to the Hellman-Feynman theorem. However, this is only applicable to fully variationally optimized wave functions. In the special case of SCF-type wave functions, the orbitals must be expanded in a complete one-electron basis set. This is never done in practice and, since one-electron basis functions are "attached" to the nuclei (and do not form a complete set), more terms arise in the expression for the gradient $\mathbf{g}$:

$$\mathbf{g} = \frac{dE}{d\mathbf{R}} = \langle\Psi|\frac{\partial\hat{H}}{\partial\mathbf{R}}|\Psi\rangle + 2\langle\frac{\partial\Psi}{\partial\mathbf{R}}|\hat{H}|\Psi\rangle, \tag{2.2}$$

where $\mathbf{R}$ are the nuclear coordinates [21]. In this equation, the first term is the Hellman-Feynman force and the second one is called the *wave-function force*, or the Pulay force. The latter reflects the dependence of the basis functions on the positions of the nuclei. The Hellman-Feynman force is easy to compute since the Hamiltonian derivative with respect to R_i is a one-electron operator. On the other hand, the Pulay force computation is more demanding, as it

requires the derivatives of molecular integrals as well as the derivatives of the density matrix (orbital coefficients). For a general wave function, which may depend on both variational and non-variationally determined parameters **c**, the energy can be written as follows [27]:

$$E = E(\mathbf{R}, \mathbf{c}(\mathbf{R})), \tag{2.3}$$

and the parameters are found as solutions of some set of equations:

$$\mathbf{f}(\mathbf{R}, \mathbf{c}(\mathbf{R})) = 0. \tag{2.4}$$

Then the energy gradient is written as:

$$\mathbf{g} = \frac{\partial E}{\partial \mathbf{R}} + \frac{\partial E}{\partial \mathbf{c}} \frac{\partial \mathbf{c}}{\partial \mathbf{R}}, \tag{2.5}$$

where the first term includes explicit dependence of energy on the displacement via Hamiltonian and a fixed set of parameters, whereas the second term includes the derivatives of **c**. If all **c** are defined variationally, the second term vanishes. For instance, for the SCF-type methods **c** are the MO LCAO coefficients and only the first term survives, which is the sum of the Hellman-Feynman and the Pulay force as discussed above. For the CI methods, the CI coefficients are variationally defined, while the MO LCAO coefficients are not anymore. For non-variational methods, none of the derivatives in the second term vanishes. Nevertheless, it is possible to avoid calculating them. Consider an auxiliary functional:

$$E'(\mathbf{R}, \mathbf{c}(\mathbf{R}), \lambda(\mathbf{R})) = E(\mathbf{R}, \mathbf{c}(\mathbf{R})) + \lambda(\mathbf{R})(\mathbf{g}(\mathbf{R}, \mathbf{c}(\mathbf{R})), \tag{2.6}$$

where λ are the Lagrange multipliers. If equations (2.4) hold, E' has the same value as E and both have the identical gradients. E' can be made stationary with respect to both λ and **c**:

$$\frac{dE'}{d\lambda} = 0, \tag{2.7}$$

$$\frac{dE'}{d\mathbf{c}} = 0, \tag{2.8}$$

the first equation being equivalent to equation determining **c** (2.4). Using these equations we get the gradient as:

$$\mathbf{g} = \frac{\partial E'}{\partial \mathbf{R}} = \frac{\partial E}{\partial \mathbf{R}} + \lambda \frac{\partial f}{\partial \mathbf{R}}. \tag{2.9}$$

Thus, no geometric derivatives of **c** are needed. However, for each non-variational parameter, an additional equation has to be solved.

The same philosophy is applied for computing higher-order geometric derivatives of the electronic energy. This approach is known as *analytical* since all the equations derived are in principle exact. For most electronic structure methods, analytical expressions for the gradients and Hessians have been derived (e.g. in work [28]). Nevertheless, the derivatives are sometimes computed numerically using finite-difference schemes, which are not exact and computationally expensive.

Chapter 3

Potential energy surfaces

3.1 General consideration

As we have seen before, to study the motion of the nuclei within the Born-Oppenheimer approximation, one needs to construct the PES for a selected electronic state in the whole range of nuclear coordinates **R** and then to solve the nuclear Schrödinger equation. Since both operations are mathematically and technically non-trivial, a number of further simplifications have been introduced to study the motion of the nuclei.

First, we note that for many practical purposes only small regions of PES are sufficient. Since molecules are known to dissociate to non-interacting fragments, with the increase in separations between the nuclei $V(\mathbf{R})$ asymptotically converges towards a constant value. Practically, the convergence is reached at modest values of interatomic separations. Thus, only within this range should the PES be determined explicitly. On the other hand, at zero nuclear separation $V(\mathbf{R})$ in infinite due to the singularity of the Coulomb nuclear-nuclear repulsion. Between the asymptotic limit and the infinity, there may be special points on the PES, that is the points where the gradient with respect to **R** (known as *molecular gradient*) is zero: $\mathrm{g} = \nabla_{\mathbf{R}} V(\mathbf{R}) = 0$. Since $V(\mathbf{R})$ is potential energy for the nuclei, molecular gradient taken with the opposite sign represents classical forces acting on the nuclei. It is known from the experiment, that most molecules are characterized by a well-defined stable geometric shape or several distinct shapes. This means that nuclear wave function is localized in the vicinity of the PES minimum where the nuclei are trapped. Mathematically, a minimum is distinguished from other extrema by the condition that all eigenvalues of the second derivatives matrix are positive. This matrix is traditionally referred to as *molecular Hessian*. The position of the PES minimum is known as *equilibrium geometry*, $\mathbf{R}_{\mathrm{e}}$. This name reflects the analogy with classical mechanics, in which $\mathbf{R}_{\mathrm{e}}$ would be a stable equilibrium point.

Having found the PES minimum, one can use equilibrium geometry to separate rotational degrees of freedom using the Eckart conditions [29] and solve the rotational problem in the rigid rotor approximation. Note that Eckart separation is not exact. The remaining degrees of freedom are called *internal*, or *vibrational*. Since the nuclei are trapped in a small region near $\mathbf{R}_{\mathrm{e}}$, the PES in the vicinity can be approximated by the harmonic potential [30]. Then the vibrational Schrödinger equation is solved exactly and the corresponding vibrational wave function is a simple product of harmonic-oscillator wave functions, each corresponding to a

normal vibration. Thus, the rovibronic molecular wave function is approximated as a product of electronic wave function evaluated at $\mathbf{R}_e$, harmonic vibrational wave function and the rigid rotor rotational one:

$$\Psi \approx \Phi(\mathbf{R}_\mathrm{e})\chi_\mathrm{HO}\chi_\mathrm{RR}. \tag{3.1}$$

Such a crude approximation turns out to be surprisingly successful for describing molecular properties, including vibrational and rotational spectra, NMR-shieldings, dipole moments, polarizabilities and so. Of course, more elaborate models can be build, but everything starts with locating the PES minimum. The distinct minima on the PES correspond to conformations and isomers of the molecule. From topological point of view, there is no principle difference between the former and the latter, but they are traditionally distinguished, whether the chemical bonds need to be broken and formed (isomers) or not (conformations) for the transition to happen.

The other type of the PES special point having physical sense is the first order saddle point, at which only one molecular Hessian eigenvalue is negative, whereas the others are positive. It is a maximum in one direction and a minimum in all the remaining ones. The former direction is defined by the Hessian eigenvector (normal coordinate), corresponding to the negative eigenvalue (and imaginary vibrational frequency, respectively). The first-order saddle point of the PES is called the *transition state* (TS) and is the key entity of the transition state theory (TST) [31]. This theory assumes that the chemical reaction, that is a transition from one PES minimum to another, proceeds over the energy barrier along the lowest energy path (or intrinsic reaction coordinate [32]). The highest point of the path is the TS. In other words, TS divides a space into the reactant and product regions with a surface normal to the reaction coordinate [31]. In the conventional TST, knowing the energy barrier – the energy difference between the TS and the reactants – and their partition functions is enough to calculate the rate coefficient. TST and its modifications is the essential part of modern chemical kinetics [33].

We have seen, that by restricting the PES exploration to locating minima and TS, known as *geometry optimization* [56], and finding reaction paths, it is possible to solve many chemical problems, including the calculation of molecular properties and studying mechanisms and kinetics of chemical reactions.

The second simplification in solving the nuclear problem is replacing the quantum equations of motion with the classical ones, for instance, in the Hamiltonian form [34]:

$$\dot{\mathbf{q}} = \frac{\partial H}{\partial \mathbf{p}}, \tag{3.2}$$

$$\dot{\mathbf{p}} = -\frac{\partial H}{\partial \mathbf{q}}, \tag{3.3}$$

$$\tag{3.4}$$

where $\mathbf{q}$ and $\mathbf{p}$ are generalized coordinates and momenta and H is the classical Hamilton function. In the absence of external forces, it is the sum of the classical kinetic energy T, depending only on the momenta, and the potential energy V, depending solely on the coordinates. Thus, the nuclei are dealt with as point particles, and the system moves along the trajectories in *phase space* spanned by the $\mathbf{q}$ and $\mathbf{p}$. The method is known as *molecular dynamics* [57]. The poten-

tial energy $V(\mathbf{R})$ is calculated solving the electronic Schrödinger equation and, as mentioned before, molecular gradient taken with the opposite sign serves as forces acting on the nuclei. Therefore, such trajectories are often called *semiclassical*, since they use forces obtained from electronic structure (i.e. quantum) calculations. Up to this point, we have been considering the time-independent Schrödinger equation. The time-dependent equation reads as follows:

$$i\hbar\frac{\partial}{\partial t}\chi_m^n(\mathbf{R};t) = [\hat{T} + V^n(\mathbf{R})]\chi_m^n(\mathbf{R};t), \tag{3.5}$$

where χ_m^n corresponds to rovibrational state m within electronic state n, to which the PES $V^n(\mathbf{R})$ corresponds. Time is not coupled with spatial coordinates in equation (3.5). For that reason, Born-Oppenheimer separation is also valid for the time-dependent case as well. Solving equation (3.5) is known as quantum dynamics of the nuclei. Since classical equations of motion are always time-dependent, the question arises whether molecular dynamics can mimic the time-independent wave-functions? The answer comes from statistical mechanics: by ensemble-averaging of the classical trajectories of the nuclei, one approximates quantum dynamics, whereas static properties are obtained by both ensemble and time-averaging [35].

The physical idea behind introducing molecular dynamics is similar to the idea behind the Born-Oppenheimer approximation: both exploit significant masses of the nuclei. In molecular dynamics, it is assumed that wave packets corresponding to the nuclei are so narrow that the density of them $|\chi_m^n(\mathbf{R};t)|^2$ can be represented by the product of Dirac delta-functions centered on the instantaneous positions of the nuclei [36] $\prod_{i=1}^{N}\delta(\mathbf{R}_i - \mathbf{R}_i(t))$. Then the expectation value of the nuclei position operator in the classical limit ($\hbar \to 0$) is reduced to the instantaneous position:

$$\int \chi_m^n(\mathbf{R};t)^*\mathbf{R}\chi_m^n(\mathbf{R};t)d\mathbf{R} \to \mathbf{R}(t), \tag{3.6}$$

that is, nuclei move as classical point masses.

Introduction of molecular dynamics significantly simplifies the solution of the nuclear problem at the expense of some accuracy. Molecular dynamics allows obtaining qualitatively valid results for a wide-spectrum of molecular and condensed-phase systems, intractable by quantum dynamics. In addition, molecular dynamics framework leaves the space for approximate incorporation of quantum effects, such as tunneling via path-integral dynamics [37] and some other techniques [38, 39]. However, these methods are beyond the scope of this thesis.

Finding the reaction coordinate, classical and quantum dynamics of the nuclei can be treated on same footing using the generalized Hamilton-Jacobi (HJ) framework [42]. Consider the functional:

$$I[\mathbf{q}(\tau)] = \int_{\tau_0}^{\tau} F(\mathbf{q}, \dot{\mathbf{q}}, \tau')d\tau', \tag{3.7}$$

where τ is an independent parameter, $\mathbf{q}$ are generalized coordinates and $\dot{\mathbf{q}}$ are their derivatives with respect to τ. For this functional, the HJ-like equation is

$$\frac{\partial I}{\partial \tau} + \frac{1}{2}\nabla_{\mathbf{q}}^T I \nabla_{\mathbf{q}} I + V(\mathbf{q},\tau) = 0, \tag{3.8}$$

where $V(\mathbf{q},\tau)$ is a general potential.

For finding reaction path, τ is the reaction coordinate which we denote as s:

$$F(\mathbf{q}, \dot{\mathbf{q}}, s) = [\mathbf{g}(\mathbf{q})^T \mathbf{g}(\mathbf{q})]^{1/2} [\dot{\mathbf{q}}^T \dot{\mathbf{q}}]^{1/2}, \tag{3.9}$$

where molecular gradient is denoted as $\mathbf{g}(\mathbf{q})$ and the HJ equation (3.8) reduces to a simple one:

$$\mathbf{g}(\mathbf{q}) = \nabla_{\mathbf{q}} V(\mathbf{q}). \tag{3.10}$$

In this equation, $V(\mathbf{q})$ is the PES and by integrating in over s one obtains the steepest-descent curve $\mathbf{x}(s)$ connecting two PES minima via the TS.

In case of classical (or semiclassical) molecular dynamics, τ is time, t, $F(\mathbf{q}, \dot{\mathbf{q}}, t)$ is the classical Lagrangian function:

$$F(\mathbf{q}, \dot{\mathbf{q}}, t) = \frac{1}{2} \dot{\mathbf{q}}^T \dot{\mathbf{q}} + V(\mathbf{q}), \tag{3.11}$$

where $V(\mathbf{q})$ is PES. The functional $I[\mathbf{q}(t)]$ is, therefore, the classical action, $S_{class}(\mathbf{q}, t)$. Then HJ equations are simplified yielding:

$$\dot{\mathbf{q}} = \nabla_{\mathbf{q}} S_{\text{class}}(\mathbf{q}, t). \tag{3.12}$$

By solving this equation classical trajectories are be generated.

In a more complicated case of quantum dynamics, one needs to express F in terms of the wave functions transformed in a Bohmian way [43]:

$$\chi(\mathbf{q}; t) = \rho(\mathbf{q}, t)^{1/2}(\mathbf{q}, t) e^{iS(\mathbf{q},t)/\hbar}, \tag{3.13}$$

where $\rho(\mathbf{q}, t)$ is the density function for the nuclei and $S(\mathbf{q}, t)$ is action, both real-valued. Then the HJ-like equation can be shown to take the form:

$$\frac{\partial S(\mathbf{q}, t)}{\partial t} + \frac{1}{2} \nabla_{\mathbf{q}} S(\mathbf{q}, t)^T \nabla_{\mathbf{q}} S(\mathbf{q}, t) + V_{\text{eff}}(\mathbf{q}, t) = 0, \tag{3.14}$$

where $V_{\text{eff}}(\mathbf{q}, t)$ is the sum of the PES and the time-dependent *quantum potential* [43]. This equation in turn is reduced to:

$$\dot{\mathbf{q}} = \nabla_{\mathbf{q}} S(\mathbf{q}, t). \tag{3.15}$$

By solving it, one obtains *quantum trajectories*. In this formulation of quantum dynamics by Bohm, nuclei move along the trajectories which "exchange information" via the quantum potential. In principle, the evolution of their density $\rho(\mathbf{q}, t)$ must be a true quantum one.

Now, we have seen that finding reaction coordinate, (semi)classical molecular dynamics and quantum trajectories may be understood and rationalized in a uniform way using the HJ formalism. This highlights the intimate relation between the ways of exploring PES.

As we know, the concept of PES stems from quantum mechanics (i.e. the Born-Oppenheimer approximation) and, therefore, the most obvious and consistent way of obtaining it is to solve the electronic Schödinger equation. Nevertheless, there exist alternative methods for getting $V(\mathbf{R})$. The most wide-spread of them is the *force-field* method (FF), or *molecular mechanics* method (MM) [40]. This approach assumes that interaction between the nuclei can be writ-

ten as a simple analytical function of atom separations, bond lengths, torsion angles and other internal coordinates (see Chapter 4). The parameters for it are obtained from empirical data or/and from high-level theoretical calculations. The FF methods are computationally cheaper than the electronic structure ones, but are generally less accurate, the accuracy being system-sensitive. There also exist hybrid methods based on partitioning the system into regions, some of which are treated with FF, while the others with quantum mechanics [41]. This approach is called QM/MM: quantum mechanics/molecular mechanics. A detailed consideration of the FF and QM/MM techniques is beyond the scope of the thesis. As a final remark, we note that all the apparatus of PES exploration (optimization and dynamics) is applicable to the FF potentials as well as to the electronic structure ones. The differences stem from the fact that for the FF calculations obtaining energies and forces and "moving the nuclei" as well as coordinate transformations require compatible computational effort. In contrast, for the electronic structure calculations the former are much more expensive than the latter. In case of molecular dynamics, the calculations employing electronic structure theory are regularly referred to as *ab initio* molecular dynamics to distinguish them from the FF-based simulations. This terminology may be confusing, since in molecular dynamics both wave-function based and DFT methods are referred to as *ab initio*, while in quantum chemistry only the first ones.

3.2 Force-modified PES and mechanochemistry

Mechanochemistry studies chemical reactivity upon mechanical activation of molecules and condensed-phase systems. Origins of mechanical forces may be diverse: stretching with atomic-force microscope needle, ultrasound, grinding and so on [44]. Strictly speaking, to model the effect of the mechanical force on a molecule, one should consider both the substrate and the force source explicitly on the atomistic level. However, this approach is not only complicated but also lacks generality. Indeed, by sacrificing rigour to a certain extent, it may be possible to reveal widely applicable concepts.

To construct a general model for mechanochemistry, it is necessary to discard the nature of the mechanical force, considering only its direction and magnitude. Hence, additional terms connected to the force should be included into the molecular Hamiltonian. Although there has been an attempt to connect the external force to both electronic and nuclear degrees of freedom [45], it is generally assumed that the force acts on the nuclei and, as a consequence, modifies, or transforms, the PES. The resulting PES is known as *force-transformed*, or *force-modified PES* (FM-PES). The electrons are only implicitly affected via displacements of the nuclei in this approach.

There are two alternative (and closely related) approaches to study FM-PES, which differ in the way the force is formally represented: either as a geometric constraint or as an addition to the Born-Oppenheimer potential energy. The first one is known as "COnstrained Geometries simulate External Force" (COGEF) [46], whereas the other is called "External Force is Explicitly Included" (EFEI) [48]. If all but one – $\mathbf{q}_0$ – geometric parameters, that is, internal coordinates, are optimized, then there is only one non-vanishing "internal" force inside the molecule. This is equivalent to the application of the external force of the same magnitude but the opposite direction. By varying the value of $\mathbf{q}_0$ it is possible to model the effect of the external force on

the PES. This is the rationale beyond the COGEF approach.

Within the EFEI technique, FM-PES is written as follows:

$$V_{\mathrm{EFEI}}(\mathbf{R}, \mathbf{F}_0) = V(\mathbf{R}) - \mathbf{F_0 q}(\mathbf{R}), \tag{3.16}$$

where $\mathbf{F}_0$ is the external force and $\mathbf{q}$ is the internal coordinate to which the force is applied. In most applications, $\mathbf{q}$ is a bond distance between the atoms on which the force acts. Generally, there can be a sum of external force terms in equation (3.16) if there are several forces acting. This may also be the case if the force is assumed to be applied not directly to the pair of atoms, but to the fixed points in space in the vicinity of the molecule [47]. Here we will be using the simple version of the theory as expressed in equation (3.16).

Since the force is the negative gradient of the potential with respect to the corresponding geometric parameter, $\mathbf{F}_0$ and $\mathbf{q}_0$ are conjugate variables in terms of the Legendre transformation [48]. It can be shown that at the stationary conditions the COGEF FM-PES is a Legendre-transform of the EFEI PES:

$$V_{\mathrm{EFEI}} = V_{\mathrm{COGEF}}(\mathbf{q}_0) - \mathbf{F}_0\mathbf{q}_0. \tag{3.17}$$

The structure optimized under $\mathbf{F}_0$ has the conjugate geometry parameter equal to $\mathbf{q}_0$ and vice versa: structure optimized with $\mathbf{q}_0$ constrained has the only non-vanishing "internal" force equal to $\mathbf{F}_0$. Thus, applying either the IFEI or the COGEF approach allows using well-developed PES exploration machinery straightforwardly to study FM-PES and to simulate mechanochemical processes, since no modifications of electronic structure theory are involved.

An important simple model in mechanochemistry is the Bell's theory, which regards the external force as a perturbation to the PES and, consequently, avoids the construction of FM-PES altogether [49]. Up to the second order in perturbation, the reaction barrier $\Delta V(\mathbf{F})$ and the geometry of the minimum $\mathbf{R}_{\mathrm{e}}(\mathbf{F})$ and the TS $\mathbf{R}_{\mathrm{TS}}(\mathbf{F})$ are found as follows:

$$\Delta V(\mathbf{F}) = \Delta V(0) - \mathbf{F}(\mathbf{R}_{\mathrm{TS}}(0) - \mathbf{R}_{\mathrm{e}}(0)) - \frac{1}{2}\mathbf{F}^T(\mathbf{H}_{\mathrm{TS}}^{-1} - \mathbf{H}_{e}^{-1})\mathbf{F}, \tag{3.18}$$

$$\mathbf{R}_{\mathrm{e}}(\mathbf{F}) = \mathbf{R}_{\mathrm{e}}(0) + \mathbf{H}_{e}^{-1}\mathbf{F}, \tag{3.19}$$

$$\mathbf{R}_{\mathrm{TS}}(\mathbf{F}) = \mathbf{R}_{\mathrm{TS}}(0) + \mathbf{H}_{\mathrm{TS}}^{-1}\mathbf{F}. \tag{3.20}$$

In these equations, subscripts $_{\mathrm{e}}$ and $_{\mathrm{TS}}$ denote the PES minimum (equilibrium) and the TS, whereas (0) and $(\mathbf{F})$ mean that the entity corresponds to the absence of force or force $\mathbf{F}$ respectively. $\mathbf{H}$ are the Hessian matrices calculated without the force. In the linear approximation – the original Bell's theory – only the terms not involving the Hessians survive in eqs. (3.18). Thus, the force does not change the geometry of the minimum and the TS, but changes only the barrier, which depends on the force linearly. The extended Bell's theory [50] eqs. (3.18) exhibits a more complicated barrier dependence on the force. Besides, it explains the "Hammond" effect, that is, the shift in the positions of the stationary points. On the basis of the linear expression for the barrier, the rule for a single bond stretch follows immediately: if the bond length in the TS is longer than in the minimum, application of the pulling force reduces the barrier (accelerates the reaction) and vice versa.

We see that the Bell's theory provides much useful information about mechanochemistry

without explicit construction of FM-PES. To compare the processes with and without mechanical activation, it is enough to locate the minimum and the TS on the PES. If geometric configurations are known and the Hessians are available, mechanochemical properties are readily calculated as analytical functions of the force applied. However, the Bell's theory is a variant of the TST and can not be coupled with molecular dynamics unlike a more general EFEI approach. Moreover, it is restricted to the small- and medium-magnitude mechanical forces.

In reality, the force dependence may be rather complicated as in the case of the disulfide bond breaking followed by nucleophilic substitution [51]. Under small forces, there is an increase in the rate with the growth of the force. However, at the certain point, mechanical tension forces the system into a different conformation, providing steric protection of the disulphide bond from the nucleophilic attack. Consequently, the rate growth decreases. For such a complicated case, the COGEF or the EFEI approaches should be used, being the compromise between applicability and rigour.

Chapter 4

Coordinate systems and transformations

4.1 General consideration

The choice of coordinate system is crucial for the performance of PES exploration techniques in terms of reliability, accuracy and computational efficiency. Geometry optimization is performed in the $3N$-dimensional *configuration space* $\{C\}$ formed by the positions of the nuclei. Molecular dynamics finds the trajectories in the *phase space* $\{P\}$ which is spanned by the positions and the conjugate momenta, or equivalently, velocities [52]. $\{P\}$ is thus a $6N$-dimensional space and $\{C\}$ is the subspace of $\{P\}$. Configuration space should not be confused with the 3-dimensional physical space in which molecular geometry may be visualized. Sometimes configuration and phase space are reduced on purpose by implying constraints [53, 54]. Then the exploration is performed on the appropriate subspaces of $\{C\}$ or $\{P\}$. Since PES is translationally and rotationally invariant, for locating its special points, that is geometry optimization, it is convenient to separate translation and rotation of the molecule as a whole and to work in $3N - 6(5)$-dimensional configuration space. In molecular dynamics this is not frequently done since, for example, rotational-vibrational couplings may be of interest in the simulation. Moreover, the Eckart separation of rotation [29] is not exact and thus performing it in dynamics could lead to losing of some important physical details. In the special case of ions in magnetic fields [55] even the centre-of-mass motion separation is not exact and should not be performed in dynamics. This is, however, beyond the scope of the current discussion.

The PES is obtained by solving electronic Schrödinger equation (or by the force-field method not considered here) which requires Cartesian coordinates of the nuclei in the laboratory or centre-of-mass frame $\mathbf{x}$ as input. Therefore, $\mathbf{x}$ is the default choice as well as the starting point for further transformations. We can formulate the following general requirements for the coordinate system:

1. it should reflect the physics (and chemistry) of the system;
2. selected coordinates should span the whole configuration space $\{C\}$;
3. coordinate transformations should be readily available, accurate and computationally non-demanding.

Hereafter we will refer to them as *physical*, *mathematical* and *computational* requirements.

First, we consider the physical requirements imposed on the coordinate systems by geometry optimization. Local optimization methods are based on power-series expansion of PES in the vicinity of some point [56]. Physically, PES is invariant to any coordinate transformation but its expansion may sometimes be simplified. It is favourable that in the optimal frame the harmonic couplings (off-diagonal elements of the Hessian) and anhormonicities (and higher order terms) are as small as possible compared with diagonal terms and first derivatives. Then the gradient (and Hessian)-based techniques will give the longer steps improving the efficiency. The *internal coordinates* satisfy this requirement quite well [57]. These coordinates reflect chemical bonding pattern of the molecules and are defined as bond lengths, valence and dihedral angles (torsions and out-of-plane bends) - referred to as *primitive internal coordinates* - and their linear combinations. Another advantage of internal coordinates is that they provide a natural framework for the configuration space partitioning which is used for locating transition states on the reduced PES (RPES) [58, 59] or for performing constraint optimizations [53]. In RPES approaches one or a few internal coordinates are selected as able for describing the reaction coordinate and treated differently from the rest. Since chemical reactions or conformational changes involve bond-breaking and/or rotation of functional groups it is difficult to perform RPES searches without internal-coordinate analysis. *Normal coordinates* are defined as eigenvectors of the Cartesian mass-weighted molecular Hessian. If the harmonic vibrational problem is solved in internal coordinates then the resulting vibrational modes are described by *curvilinear normal coordinates* [60, 61]. For the Newton's optimization method or other methods assuming the knowledge of the molecular Hessian (curvilinear) normal coordinates are the natural choice.

On-the-fly BOMD is also based on the local Taylor-expansion of $V(\mathbf{R})$ (see Chapter 5). Therefore, the considerations above are valid for this type of PES exploration techniques. However, classical equations of motion impose additional requirements on the coordinate system, namely the equations should exhibit certain symmetries. Time-reversibility and space uniformity, which impose energy and linear momentum conservation respectively, are trivially valid for any frame, while not all the coordinate systems are rotationally invariant. Thus, angular momentum may not be conserved violating the requirement the space anisotropy. For instance, equations of motion in normal coordinates are not rotationally invariant and the Hessian-based integrators employing them suffer from poor conservation of angular momentum [62, 63]. This problem is dealt with either by projecting the forces onto the invariant space [63] or by using Cartesian coordinates [64] which preserve all the symmetries. The latter is more consistent but more difficult to implement and requires a greater computational effort. As will been shown in Chapter 5, for most systems larger than 10 atoms, gradient-based integrators are computationally superior to the Hessian-based ones and most applications are currently performed using the former. This means that the properties of internal coordinates, so convenient for geometry optimization - small harmonic couplings and anharmonicities - are not useful in dynamics. Although several consistent formulations of MD in internal coordinates have been proposed [65, 66] they do not show any significant advantages (if any) over integration in the Cartesian coordinates which is the choice for most existing algorithms and computer programs. Often, mass-weighted Cartesian coordinates are used for integrating classical equations of motion which assumes multiplication or division of the vectors (Coordinates, gradients, velocities) by the square root of the appropriate nuclear mass. Although additional operations are introduced,

mass-weighting simplifies the equations of motion, eliminating masses from them.

To begin the consideration of mathematical requirements we define primitive internal coordinates $\mathbf{q}$ as analytical functions of $\mathbf{x}$:

$$\mathbf{q} = \mathbf{q}(\mathbf{x}). \tag{4.1}$$

Then we introduce the Jacobian, or *Wilson's B-matrix* [30], necessary to perform coordinate transformations between the Cartesian coordinates $\mathbf{x}$ and primitive internal coordinates $\mathbf{q}$:

$$B_{ij} = \left.\frac{\partial q_i(x)}{\partial x_j}\right|_{x=x_0}. \tag{4.2}$$

For infinitesimal displacements $\delta q_i = B_{ij}\delta x_j$, while finite displacements $\Delta\mathbf{q}$ and $\Delta\mathbf{x}$ are not related linearly anymore, since generally $\mathbf{q}(\mathbf{x})$ is a non-linear function (as in case of bond lengths, valence angles and torsions). For all widely used primitive coordinates analytical definitions as well as $\mathbf{B}$ elements are known [30, 67]. If the coordinates $\mathbf{q}$ are related to some other set of internals $\mathbf{Q}(\mathbf{x})$ by a linear transform

$$\mathbf{Q} = \mathbf{A}^T\mathbf{q}, \tag{4.3}$$

then we have

$$\mathbf{B}_Q = \mathbf{A}^T\mathbf{B}. \tag{4.4}$$

Obviously, for primitive internal coordinates, $\mathbf{A}$ reduces to a unit matrix. Further on, we will use $\mathbf{Q}$ as any set of internal coordinates including $\mathbf{q}$ as a special case.

As mentioned above, $\mathbf{Q}$ must span the whole configuration space $\{C\}$, namely, any vector in C_i (a particular geometric configuration) must be able to be expressed as a linear combination of Q_j:

$$C_i = \sum_{j=1}^{M} d_{ij}Q_j, \tag{4.5}$$

where d_{ij} are the expansion coefficients and M is the number of internal coordinates. If (4.5) holds and $\mathbf{Q}$ are linearly independent then they form a basis in $\{C\}$ [68]. In such cases, $M = 3N - 6(5)$ and the set $\mathbf{Q}$ are called *non-redundant*. Equation (4.5) may also hold for linear-dependent, or *redundant* coordinates ($M > 3N - 6(5)$). Although they do not form a basis and lack some special properties they are applicable for practical purposes of geometry optimization.

Internal coordinates are either hand-picked or selected automatically. Automated procedures are generally based on finding the bonds between the atoms using covalent or van der Waals radii, the angles and dihedrals formed by these bonds. Internal coordinates are defined either for the whole molecule at once [69, 67] or fragment-wise [70, 71]. Decius have shown that by taking proper combinations of the four basic types of primitive internal coordinates it is always possible to obtain a set spanning the configuration space [72]. Nevertheless, most sets of primitive internal coordinates $\mathbf{q}$ [67, 74] as well as their predefined linear combinations (such as *natural internal coordinates* [73]) used in practice do not span $\{C\}$ by construction. It is possible to check whether equation (4.5) holds by inspecting matrix $\mathbf{G} = \mathbf{B}_Q\mathbf{B}_Q^T$: if it has exactly $3N - 6(5)$ non-zero eigenvalues then $\mathbf{Q}$ spans the configuration space [75]. Eigenvectors of $\mathbf{G}$

corresponding to non-zero eigenvalues are known as *delocalized internal coordinates* and are extensively used in geometry optimizations [76]. A special case of the non-redundant primitive set the is the *Z-matrix* which reflects the atom connectivity of the molecule [77]. Although a properly constructed Z-matrix can facilitate optimization, it is tedious to build manually, while automatically generated Z-matrices are often poor. Therefore, Z-matrix method is now seldom used as a working framework, finding, however, other applications (see section 6.2).

The **G**-matrix eigenvalue-test shows whether the coordinate set is complete only for the geometric configuration at which internal coordinates were defined [72, 78]. At different configurations the same set of internal coordinates may loose this property and fail to span $\{C\}$. Nevertheless, the definitions of most internal coordinates **Q** are based on much chemical and physical sense and, as a consequence, rarely fail to span the configuration space, especially when local optimization is performed. Yet it is still useful to check if this is true.

As far as *computational* requirements to the coordinate system are considered, we point out that using Cartesian frame eliminates nearly all coordinate transformations at all since the energy and its derivatives are almost always evaluated in Cartesian coordinates. This is frequently done in molecular dynamics and force-field calculations. Although **x** does not reflect the bonding pattern in molecules and it takes more steps to converge the optimization, the computational effort saved by avoiding coordinate transformations is often more significant [79]. This is, however, not the case for electronic structure calculations for which evaluation of energy and its derivatives is orders more computationally expensive than all other operations.

The relationships for the energy gradient **g** and the Hessian **H** in the Cartesian **x** and any other coordinates **Q** are as follows [67]:

$$\mathbf{g}_x = \mathbf{B}_Q^T \mathbf{g}_Q, \tag{4.6}$$

$$\mathbf{H}_x = \mathbf{B}_Q^T \mathbf{H}_Q \mathbf{B}_Q + \mathbf{K}, \tag{4.7}$$

$$K_{jk} = \sum_i [\mathbf{g}_Q]_i \frac{\partial^2 Q_i}{\partial x_j \partial x_k}, \tag{4.8}$$

and

$$\mathbf{g}_Q = (\mathbf{B}_Q^T)^+ \mathbf{g}_x, \tag{4.9}$$

$$\mathbf{H}_Q = (\mathbf{B}_Q^T)^+ (\mathbf{H}_x - \mathbf{K}) \mathbf{B}_Q^+. \tag{4.10}$$

In these equations $^+$ denotes a generalized inverse (or inverse for the square matrices) and the term **K** arises because of the chain rule [67]. At PES extrema, gradient is zero and **K** vanishes. The same occurs if linearized coordinates are used but this time because of zero second derivatives of **Q**. Moreover, if linearized coordinates are orthogonal - such as the normal coordinates - then the Jacobian is orthogonal and there is no need to build the inverse explicitly which is the most computationally expensive procedure here. Nevertheless, above we have pointed out good reasons for using *curvilinear* coordinates such as internal coordinates. Equations (4.6) and (4.9) are exact and since analytical expressions for internal coordinates and their derivatives are well known [67, 80] there are no principle difficulties in performing these transformations.

4.2 Coordinate back transformation

The situation is quite different for transforming the displacements. Of course, transforming $\Delta\mathbf{x}$ to $\Delta\mathbf{Q}$ is trivial because $\mathbf{Q}(\mathbf{x})$ is defined analytically. However, the same is not true for the functional dependence $\mathbf{x}(\mathbf{Q})$ due to non-linearity. Yet if internal coordinates are used, the step is defined in this frame and, thus, the transformation of $\Delta\mathbf{Q}$ to $\Delta\mathbf{x}$ needs to be done:

$$\mathbf{Q}(\mathbf{x}_0 + \Delta\mathbf{x}) = \mathbf{Q}_0(\mathbf{x}_0) + \Delta\mathbf{Q}. \tag{4.11}$$

In this equation, $\mathbf{x}_0$ and $\mathbf{Q}_0$ are initial values, $\Delta\mathbf{Q}$ is known and $\Delta\mathbf{x}$ is to be found. This is in fact a system of non-linear algebraic equations known as *coordinate back transformation* [81]. These equations do not have an analytical solution and the transformation is performed approximately, being one of the most expensive coordinate transformation operations. By contrast, for linearized coordinates, back transformation is exact and trivial.

We here assume that $\mathbf{Q}$ is a nonredundant and complete set. Before discussing the techniques for back transformation, we introduce the *rigidity for displacement* of the coordinate system [82], defined as the norm of the residual of the step in internal coordinates obtained by back-transformation divided by the norm of the step predicted by the optimizer. Obviously, for redundant coordinates, rigidity may be nonzero and thus may serve as a measure of redundancy. Therefore, even if the step is found in redundant coordinates, an auxiliary non-redundant set must be involved in the back transformation to check its convergence properly.

4.2.1 Iterative back transformations

Iterative back transformation (IBT) is performed according to the equation:

$$\mathbf{x}_{k+1} = \mathbf{x}_k + \mathbf{B}_k^{+}[\mathbf{Q}_0 + \Delta\mathbf{Q} - \mathbf{Q}_k] \tag{4.12}$$

where $\Delta\mathbf{Q}$ is the step defined by the optimizer and k is the iteration counter. IBT is analogues to the Newton-Raphson method for solving the systems of non-linear equations, requiring reevaluation of $\mathbf{B}$ and its generalized inverse at each iteration. A simplified iterative back transformation (SIBT) uses one $\mathbf{B}^{+}$ evaluated at $\mathbf{x}_0$ throughout.

4.2.2 Z-matrix assisted transformation

Baker and Pulay proposed an alternative method for performing the back transformation which circumvents expensive inverse computation [81]. Their algorithm is based on finding the Cartesian displacements using a Z-matrix which is explicitly constructed for this purpose, while the step is itself taken in the delocalized internal coordinates. The new values of the internals are generated, compared to the predicted step and improved in an iterative procedure. This technique avoids building the (pseudo)inverse altogether.

4.2.3 High-order path expansion

The HOPE method is based on a reformulation of the back transformation problem (see Article II). It introduces the path length variable s. We assume that during the step internal coordinates

are changing linearly:

$$\mathbf{Q}(s) = \mathbf{Q}_0 + \Delta\mathbf{Q}s. \tag{4.13}$$

Therefore the path in Cartesian coordinates is defined by solving a set of differential equations:

$$\mathbf{Q}(\mathbf{x}(s)) = \mathbf{q}_0 + \Delta\mathbf{q}s. \tag{4.14}$$

Instead of integrating eq. (4.14) numerically we look for the solution $\mathbf{x}(s)$ in the form of a power series:

$$\mathbf{x}(s) = \mathbf{x}_0 + \mathbf{x}_1 s + \mathbf{x}_2 s^2 + \dots \tag{4.15}$$

By Taylor-expanding both sides of Eq. 4.14 in s (assuming that $\mathbf{Q}(\mathbf{x})$ is an analytical function at $\mathbf{x}_0$) we obtain the following set of equations:

$$\mathbf{B}_Q\mathbf{x}_1 = \Delta\mathbf{Q} \tag{4.16}$$

$$\mathbf{B}_Q\mathbf{x}_2 = -[\mathbf{Q}(\mathbf{x}_0 + \mathbf{x}_1 s)]_2 \tag{4.17}$$

$$\mathbf{B}_Q\mathbf{x}_3 = -[\mathbf{Q}(\mathbf{x}_0 + \mathbf{x}_1 s + \mathbf{x}_2 s^2)]_3 \tag{4.18}$$

$$\dots \tag{4.19}$$

where the square brackets mean that we extract a certain order (in s) of the value in the brackets. This is a triangular system of equations, where the x_i's can be determined order by order. The HOPE method requires only one evaluation of the generalized inverse of $\mathbf{B}_Q$. The derivatives are evaluated in primitive internal coordinates but the method as a whole can be applied to any linear combination of them. In contrast to other methods, the HOPE method finds not only the Cartesian coordinates corresponding to the displacement but also a path between the initial and the final positions, expressed in a simple analytical form of a power series.

4.2.4 Performance of transformation schemes

We compare the performance of the IBT, SIBT, and HOPE methods for the first geometry step (of length 0.5 a.u. and 1 a.u., with angles in radians) in the geometry optimization of the seven medium-sized and large molecules depicted in Fig. 4.1: cholesterol ($C_{27}H_{46}O$), a Si_{40} cluster [83], the cubic conformation of a protonated water cluster $(H_2O)_{20}H^+$ [84], endofullerene $H_2O@C_{60}$ with an off-center water molecule [85], a pyridine–water cluster $(C_5H_5N)_2(H_2O)_6H^+$ [86], dibenzo-18-crown-6 ($C_{20}H_{24}O_6$), and valinomycin ($C_{54}H_{90}N_6O_{18}$). All electronic-structure calculations were performed using Kohn–Sham/BLYP/6-31+G* theory. Optimization method is the quasi-Newton technique by Bakken and Helgaker [67] using primitive redundant internal coordinates $\mathbf{q}$. Non-redundant delocalized internal coordinates [76] along with Cartesian ones are used to control the convergence of back-transformation. Convergence is declared when the root-mean-square change in the coordinates is less than 10^{-6} and when this change differs by less than 10^{-12} from that of the previous iteration (or order of expansion for the HOPE method). High-order derivatives of the internal coordinates for the HOPE transformation have been calculated using automatic differentiation technique [87].

The main results are summarized in the Table 4.1, where we list the Taylor expansion order for the HOPE calculations and the number of iterations for the IBT and SIBT calculations; in

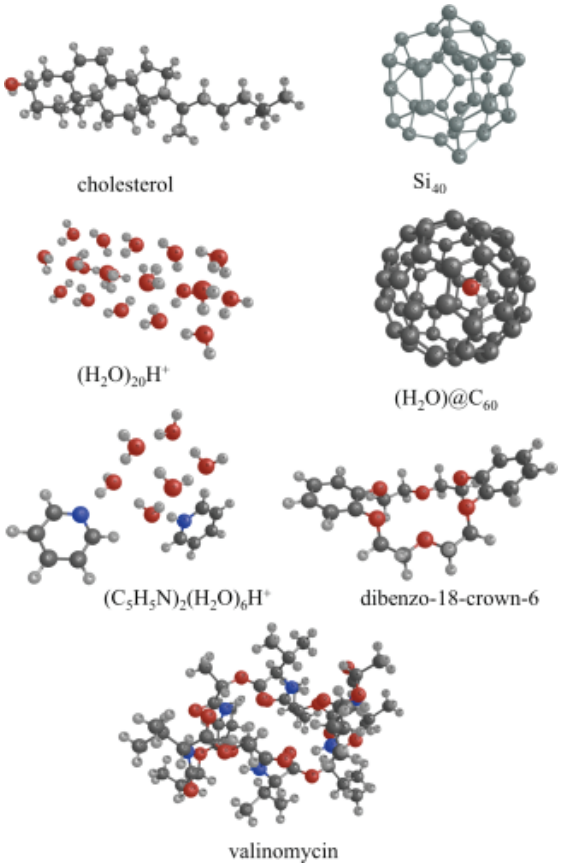

Figure 4.1: Optimization test set.

Table 4.1: Performance of the IBT, SIBT and HOPE methods for six molecules of N internal coordinates and for two step lengths. For each calculation, we list n/m where n is the number of $\mathbf{B}^+$ evaluations and m is the number of linear systems solved to achieve convergence. In the HOPE method, one linear system is solved for each order in the expansion; in the IBT and SIBT methods, one linear system is solved at each iteration.

	N	Step length 0.5 a.u.			Step length 1 a.u.		
		HOPE	SIBT	IBT	HOPE	SIBT	IBT
cholesterol	712	1/7	1/10	5/5	1/8	1/12	6/6
Si_{40}	1977	1/6	1/7	6/6	1/6	1/7	5/5
$(H_2O)_{20}H^+$	441	1/8	1/18	6/6	1/9	1/16	6/6
$H_2O@C_{60}$	1138	1/9	1/7	5/5	1/10	1/9	5/5
$(C_5H_5N)_2(H_2O)_6H^+$	260	1/13	1/44	6/6	1/19	2/70+18 [a]	6/6
dibenzo-18-crown-6	398	1/9	1/13	5/5	1/9	1/13	6/6
valinomycin	1525	1/7	1/9	5/5	1/7	1/9	5/5
total $\mathbf{B}^+$ evaluations		7	7	38	7	8	39

[a] For this system SIBT fails to converge for step length 1 a.u. The step is split into 2 substeps 0.5 a.u. each for which SIBT converges in 70 and 18 iterations respectfully.

the following, we shall refer to both 'expansion orders' (HOPE) and 'iteration' (IBT and SIBT) quantities as 'iterations'.

The IBT method uses fewest iterations to achieve convergence; moreover, its performance does not depend strongly on the molecular system or on the step length. The HOPE method also converges rapidly but it is slightly more sensitive to system and step length. Except for the pyridine-containing cluster, expansions up to order nine are sufficient (the pyridine system requires orders 13 and 19 for $s = 0.5(a.u.)$ and $s = 1.0(a.u.)$, respectively). The SIBT method exhibits the poorest convergence, requiring 36–46 iterations for $(C_5H_5N)_2(H_2O)_6H^+$ and $s = 0.5$. For $s = 1.0$, the SIBT method fails to converge and two steps of $s = 0.5(a.u.)$ are instead taken, each requiring a separate $\mathbf{B}^+$ evaluation.

Thus, the HOPE back transformation has proven to be a reliable procedure, superior to SIBT. Moreover, since the time-limiting step is the evaluation of pseudo-inverse of $\mathbf{B}$ the HOPE is more efficient than the IBT scheme, requiring only one evaluation of $\mathbf{B}^+$.

Chapter 5

Born-Oppenheimer molecular dynamics

5.1 Definitions and extended Lagrangian formulation

As a branch of theoretical chemistry *direct dynamics* is defined as "the calculation of rates or other dynamical observables directly from electronic structure information, without the intermediacy of fitting the electronic energies in the form of a potential energy function" [88]. In particular, direct Born-Oppenheimer molecular dynamics (BOMD) assumes integration of the classical equations of motion for nuclei calculating electronic energies and forces on-the-fly. It is thus different from the methods using preconstructed PES, which are beyond the scope of the thesis but described elsewhere (e.g. in the review [31]). Direct BOMD is a black-box approach which is more suitable for bigger systems as it automatically samples the PES regions of interest.

Direct BOMD can be introduced via the generalized Lagrangian approach [89, 90]. Let $\mathbf{x}$ be the coordinates of the nuclei and suppose that $\boldsymbol{\rho}$ describes the electronic degrees of freedom, for example, orbital coefficients, CI vectors, density matrix etc. Then the generalized Lagrangian is:

$$L(\mathbf{x}, \dot{\mathbf{x}}, \boldsymbol{\rho}, \dot{\boldsymbol{\rho}}) = \frac{1}{2}\mathbf{m}\dot{\mathbf{x}}^2 + \frac{1}{2}\boldsymbol{\mu}\dot{\boldsymbol{\rho}}^2 - V(\mathbf{x}, \tilde{\boldsymbol{\rho}}) + k\boldsymbol{\mu}G(||\boldsymbol{\rho} - \tilde{\boldsymbol{\rho}}||), \tag{5.1}$$

In this equation, $\tilde{\boldsymbol{\rho}}$ contains further electronic variables calculated as a vector-valued function $\mathbf{F}(\mathbf{x}, \tilde{\boldsymbol{\rho}})$ and V is electronic energy. Function G is positive everywhere and zero at $||\boldsymbol{\rho} - \tilde{\boldsymbol{\rho}}|| = 0$. $\mathbf{m} = diag(m_1, m_1, m_1, m_2, m_2, m_2, ..., m_N, m_N, m_N)$ defines nuclear masses, while $\boldsymbol{\mu} = diag(\mu, ..., \mu)$, μ is a fictitious parameter, which takes the role of the mass for electronic degrees of freedom. k serves as the force constant bound to the distance between $\boldsymbol{\rho}$ and $\tilde{\boldsymbol{\rho}}$. Euler-Lagrange equations derived from (5.1) take the following form:

$$\mathbf{m}\ddot{\mathbf{x}} = -\frac{\partial V}{\partial \mathbf{x}} - \frac{\partial V}{\partial \tilde{\boldsymbol{\rho}}}\frac{\partial \mathbf{F}}{\partial \mathbf{x}} + k\boldsymbol{\mu}\frac{\partial G}{\partial \tilde{\boldsymbol{\rho}}}\frac{\partial \mathbf{F}}{\partial \mathbf{x}}, \tag{5.2}$$

$$\boldsymbol{\mu}\ddot{\boldsymbol{\rho}} = -\frac{\partial V}{\partial \tilde{\boldsymbol{\rho}}}\frac{\partial \mathbf{F}}{\partial \boldsymbol{\rho}} + k\boldsymbol{\mu}\left\{\frac{\partial G}{\partial \boldsymbol{\rho}} + \frac{\partial G}{\partial \tilde{\boldsymbol{\rho}}}\frac{\partial \mathbf{F}}{\partial \boldsymbol{\rho}}\right\}. \tag{5.3}$$

If we choose $\tilde{\boldsymbol{\rho}}$ so that it minimizes $V(\mathbf{x}, \tilde{\boldsymbol{\rho}})$ with fixed $\mathbf{x}$ and $\mu \to 0$ then Lagrangian (5.1) splits into two parts:

$$L(\mathbf{x}, \dot{\mathbf{x}})_{BO} = \frac{1}{2}\mathbf{m}\dot{\mathbf{x}}_i^2 - V(\mathbf{x}, \tilde{\boldsymbol{\rho}}), \tag{5.4}$$

$$L(\boldsymbol{\rho}, \dot{\boldsymbol{x}})_{\rho} = \frac{1}{2}\dot{\boldsymbol{\rho}}^2 + kG(||\boldsymbol{\rho} - \tilde{\boldsymbol{\rho}}||). \tag{5.5}$$

The first equations are the classical equations of motion for nuclei on the Born-Oppenheimer PES, while the second represent the propagation of the electronic structure guess, subject to variational optimization. If this requirement is relaxed and $\tilde{\boldsymbol{\rho}}$ is set equal to $\boldsymbol{\rho}$ (setting G to zero) then Lagrangian (5.1) is reduced to the Car-Parrinello Lagrangian with the only parameter μ, the fictitious electron mass:

$$L(\mathbf{x}, \dot{\mathbf{x}}, \boldsymbol{\rho}, \dot{\boldsymbol{\rho}})_{CP} = \frac{1}{2}\mathbf{m}\dot{\mathbf{x}}_i^2 + \frac{1}{2}\boldsymbol{\mu}\dot{\boldsymbol{\rho}}^2 - V(\mathbf{x}, \boldsymbol{\rho}). \tag{5.6}$$

In Car-Parrinello molecular dynamics (CPMD) [91] electronics degrees of freedom (usually, density) are not optimized but rather propagated in a classical fashion. This significantly reduces cost but leads to a deviation from the true BO PES. Recently, many approaches sharing the traits of both CPMD and BOMD have been suggested e.g. [92, 93, 94, 95, 96]. All these mixed techniques as well as 'pure' CPMD and BOMD are called direct *ab initio molecular dynamics*. In this thesis, however, only BOMD is considered within the framework defined by eqns. (5.4) and (5.5): integration of the equations of motion for nuclei and the propagation of the electronic guess.

5.2 Integration of equations of motion for nuclei

Exact integration of the classical equations of motion is only possible for two-body systems [34]. Thus, in molecular dynamics these equations for nuclei are solved approximately, in most cases - but not necessarily - numerically. As in case of approximate wave functions (see Chapter 2), approximate integrators are supposed to possess important characteristics of the exact ones. These are the symmetries and corresponding conservation laws according to Neother's theorem: time invariance (time reversibility) and energy conservation, translational invariance and momentum conservation, rotational invariance and angular momentum conservation. Another requirement follows from the Liouville theorem which states that the phase space volume is constant in time. The latter is, however, automatically fulfilled if the conservation laws are imposed. An accurate approximate integrator should thus exhibit the symmetries by construction, that is the equations should be time reversible, translationally and rotationally invariant.

The key to constructing practical integration techniques is *discretization* of the trajectory. If the exact trajectory is continuous in the phase space, any approximate trajectory - whether continuous or not - is obtained based on the idea of a finite time step.The time step Δt, which may be constant or variable, is chosen so that the potential traversed during that time is accurately represented by some local model. Consequently, the methods for integrating the classical equations of motion for the nuclei may be classified according to what model is used. The local

expansion of potential energy in Cartesian coordinates is:

$$V(\mathbf{x}) = V_o + \mathbf{g}^T \Delta\mathbf{x} + \frac{1}{2}\Delta\mathbf{x}^T \mathbf{H} \Delta\mathbf{x} + ..., \tag{5.7}$$

where V_0 is energy at $\mathbf{x}_0$, and $\mathbf{g}$ and $\mathbf{H}$ are the energy gradient and Hessian evaluated at $\mathbf{x}_0$. If $V(\mathbf{x})$ is truncated after the term linear in displacement, then one obtains gradient-based methods, if the quadratic term is retained then Hessian-based methods evolve.

For the gradient-based methods, the equations of motion reduce to [97]:

$$\mathbf{m}\ddot{\mathbf{x}} = -\mathbf{g}, \tag{5.8}$$

which may be solved by any numerical technique [98]. However, preference is usually given to the *symplectic methods*, which preserve the phase space volume and exhibit time-symmetry by construction [99]. A general scheme for integration step Δt divided into m substeps ($i = 1, 2, ..., m$) is given as follows:

$$\dot{\mathbf{x}}(t_i) = \dot{\mathbf{x}}(t_{i-1}) + b_i \Delta t \ddot{\mathbf{x}}(t_{i-1}), \tag{5.9}$$

$$\mathbf{x}(t_i) = \mathbf{x}(t_{i-1}) + a_i \Delta t \dot{\mathbf{x}}(t_i), \tag{5.10}$$

where a_i and b_i are coefficients dependent on the method. The most popular integrator is the velocity-Verlet, or leapfrog method, which is a second-order integrator [100]. Integration over one time step is performed as follows:

$$\mathbf{x}(t + \Delta t) = \mathbf{x}(t) + \dot{\mathbf{x}}\Delta t + \frac{1}{2}\ddot{\mathbf{x}}(t)\Delta t^2, \tag{5.11}$$

$$\dot{\mathbf{x}}(t + \Delta t) = \dot{\mathbf{x}}(t) + \frac{1}{2}(\ddot{\mathbf{x}}(t) + \ddot{\mathbf{x}}(t + \Delta t))\Delta t. \tag{5.12}$$

Once eq. (5.11) is solved and the new positions $\mathbf{x}(t + \Delta t)$ are found, the accelerations $\ddot{\mathbf{x}}(t + \Delta t)$ are evaluated according to (5.8). Then the velocities are updated by solving eq. (5.12). Hence, the velocity-Verlet integrator requires the only energy and force evaluation per time step. This makes the method efficient, in spite of the fact that it is not the most accurate among the symplectic integrators. Nevertheless, it has been recently demonstrated that higher-order symplectic methods may also be successfully applied for BOMD using an SCF-type electronic structure method. They exhibit excellent speed/accuracy ratio provided special techniques to estimate electronic degrees of freedom are applied [101].

For straightforward Hessian-based algorithms, the equations of motion take form:

$$\mathbf{m}\ddot{\mathbf{x}} = -\mathbf{g} - \mathbf{H}\boldsymbol{\Delta}\mathbf{x}. \tag{5.13}$$

Transformed into the Hessian eigenvector basis (normal coordinates), these equations split into $3N$ independent harmonic oscillator equations, which can be integrated analytically. Hence, this technique is a rare example of a method that provides continuous analytical trajectories (although they are still approximate) [62].

This Hessian-based algorithm has been refined [63, 102, 64] to yield the *fifth-order predictor-*

corrector method. Each time-step solution of eq. (5.13) serves as a predictor step. At the end of the step, a new energy, gradient and Hessian are calculated. With V_0, $\mathbf{g}$ and $\mathbf{H}$ at the beginning and the end of the predictor step (6 entities in total) at disposal, it is possible to construct an improved local fitted PES. If a polynomial is used for fitting, then this PES is 5th order in one direction and quadratic in all the others. Subsequently, one can reintegrate the equations of motion on the fitted PES using any standard numerical technique such as the Verlet method, breaking the step into several substeps. Since the corrector step normally results in a small displacement with respect to the predictor step, there is no need to recalculate $\mathbf{g}$ and $\mathbf{H}$ at the end of the former. Thus, the next predictor step is taken using the gradient and Hessian obtained at the end of the previous predictor step so that only the evaluation of V_0, $\mathbf{g}$ and $\mathbf{H}$ per step is required. Instead of calculating $\mathbf{H}$ from electronic structure theory every step, one can rather use Hessian update techniques [102] recalculating exact Hessians once per several steps.

For Hessian-based methods, it is more convenient to control the integration by a trust radius than by a time step. The trust radius, or trust region, defines the area of configuration space within which the model potential is believed to be valid. At each step, integration is carried out until length of the step is equal to the trust radius. Using a constant trust radius results in steps of variable time duration.

When comparing the mechanical accuracy of integration algorithms, one must consider the extent to which the conservation laws are fulfilled for one and the same time step or trust radius. It turns out that momentum is always trivially conserved, whereas angular momentum conservation depends on the choice of coordinate system. Gradient-based integrators in Cartesian coordinates preserve angular momentum. The situation with Hessian-based integrators is more complicated since coordinate transformations are involved: equations (5.13) transformed into normal coordinates lack rotational symmetry and the resulting trajectories do not conserve angular momentum. Spurious angular momentum arises in the corrector step since the coordinate system is rotated to perform the fitting. This is, however, easily cured by rotating the coordinates back after the potential has been fitted. Provided the predictor step is integrated numerically in Cartesian coordinates, this imposes angular momentum conservation for the most advanced Hessian-based algorithm.

The main concern with mechanical accuracy is energy conservation. It is convenient to distinguish between short-term and long-term conservation [103]. Long-term stability is characterized by *energy drift*, defined as the slope of the linear fit of total energy change with time $E(t)$. *Energy noise*, defined as root-mean square deviation of energy from the linear fit, is an indicator of short-term violation of the energy conservation law. Significant energy noise stems from the fact that an approximate trajectory oscillates around the exact trajectory (or generally a set of similar trajectories). Classical trajectories are subject Lyapunov instability [99],meaning that initially closely lying trajectories diverge in time exponentially. Therefore, short-range fluctuations causing energy noise can significantly change the outcome of one particular trajectory. Proper statistical averaging helps the problem. Long-term energy drift leads to systematic errors in the trajectories. It cannot easily be compensated by averaging since a decrease and an increase in the total energy do not necessarily lead to opposite effects on the computed properties.

Of course, Hessian-based models are generally more accurate as they employ a more accurate model PES. The fifth-order predictor-corrector method exhibits very low energy noise

drift especially if used with a symplectic integrator or a reliable non-symplectic one such as the Bulirsch-Stoer integrator [102]. Gradient-based method with the velocity-Verlet integrator demonstrates high energy noise but excellent long-term stability.

Finally, we need to examine computational efficiency of the techniques under consideration. Method A is more computationally efficient than method B if it generates the trajectory of the same length and with same mechanical accuracy with less amount of computations, or, in simple words, if it is faster on the same computer. Evidently, computational efficiency in BOMD is a trade-off between the number of steps and computational cost of each step. First, we note that integration of equations of motion takes negligible time relative to the evaluation of V_0, $\mathbf{g}$ and $\mathbf{H}$ from electronic structure theory. Therefore, one is practically unrestricted in manipulations with coordinates, velocities, forces etc. As a consequence, the fifth-order predictor-corrector algorithm is definitely superior to a simple Hessian-based algorithm. Indeed, the former allows increasing the step length up to an order of magnitude without any loss of accuracy [63]. Second, calculation of the exact Hessian is the most expensive task. Thus, doing so every several steps and updating in between saves much computational time without significant loss of accuracy [102]. To make a choice between the gradient-based and the Hessian-based methods in terms of efficiency, one needs to compare the cost of $\mathbf{g}$ and $\mathbf{H}$. This difference depends on the system under study, on electronic structure method involved and eventually on its implementation in the program. Nevertheless, currently even at the DFT level for systems consisting of more than 10 atoms, gradient-based velocity-Verlet method is more efficient as calculation of the Hessian becomes prohibitively expensive even when performed every fifth step [64]. For smaller systems, fifth-order predictor-corrector technique is preferable. As soon as more demanding electronic-structure methods are involved, the borderline between the two methods shifts towards even smaller systems.

To conclude, we reiterate that integration of classical equations of motion for nuclei in BOMD is mostly performed by two methods: the gradient-based velocity-Verlet and the Hessian-based fifth order predictor-corrector. The second one is more efficient for small systems, while the first one is preferable for medium-sized and large systems.

5.3 Propagation of electronic degrees of freedom

One may wonder what is the use of propagating electronic degrees of freedom in BOMD when the wave function or density is anyway to be optimized each time step. It is done in order to generate a good starting guess. If it is close enough the converged wave function (density), that is $||\boldsymbol{\rho} - \tilde{\boldsymbol{\rho}}||$ is as small as possible, then it will take less time to solve electronic Schrödinger equation. Since this is performed every time step along the trajectory, a good starting guess will improve integration efficiency. Here we shall restrict ourselves to SCF methods - namely, HF method and KS-DFT theory, and only gradient-based integrators.

Propagation of the electronic guess is formally described by eq. (5.5). In reality, this also gives rise to practical algorithms such as the one described in reference [89]. However, propagation of ρ also can and is done by alternative techniques. Within the extended Lagrangian formalism, they may be regarded as approximations to eq. (5.5) although they are not necessarily less accurate.

Historically, the general idea of simultaneous propagation of electronic and nuclear degrees of freedom was proposed by Car and Parrinello in their pioneering work on CPMD [91]. Head-Gordon and Pople applied simultaneous variation of both geometry and SCF-parameters for geometry optimization [104]. Much later, the first such an approach for BOMD, *Fock matrix dynamics* (FMD), was introduced by Pulay and Fogarasi [105] and thoroughly benchmarked by Herbert and Head-Gordon [106]. The idea behind FMD is as follows: since Fock matrix elements F_{ij} explicitly depend on nuclei positions and the latter in turn change in time smoothly along the trajectory, the evolution of the former must be well described by some continuous function. This function is assumed to be an nth-order polynomial:

$$F_{ij} = \sum_{k=0}^{n} c_k t^k, \tag{5.14}$$

the coefficients c_s being found by least-squares fitting values of converged Fock elements in m previous steps. The guess Fock matrix for step $m + 1$ is found using eq. (5.14) while the guess orbitals and density matrix are obtained by diagonalizing it. It turns out that the c_k depend neither on the time-step number nor on the Fock element indices i and j but solely on m and n. This makes extrapolation computationally negligible since the c_k are to be found only once.

Application of FMD significantly reduces the number of SCF iterations per time step [105, 106] being able to improving integration efficiency by almost a factor of two. Despite this success FMD propagation lacks time reversibility. Consequently, the error due to incomplete SCF optimization tends to accumulate, leading to significant energy drift. The problem can be quenched by tightening SCF convergence criteria, although for very long simulations drift will still occur. Anyway, the FMD guess results in less drift than converged density from the previous iteration and is not much poorer in this respect than using time-independent guess (such as the extended Hückel guess).

The problem of time reversibility was solved by Niklasson et al. who proposed the filter guess. It is also based on the least-squares fitting but on both converged entities and guesses [107]. The algorithm is applicable for Fock matrices, density matrices and so on, since it is trace-conserving. The simplest scheme is as follows:

$$\boldsymbol{\rho}_{s+1} = 2\tilde{\boldsymbol{\rho}}_s - \boldsymbol{\rho}_{s-1}, \tag{5.15}$$

where s is the time-step number, entities without a tilde are guesses, while the one with a tilde is converged. This scheme and its higher-order extensions provide significant acceleration of SCF convergence but also preserve long-scale energy conservation. Niklasson and colleagues have also developed more advanced propagation techniques including time-derivatives of $\boldsymbol{\rho}$ [101], increasing computational efficiency, and also dissipation terms [108, 109], imposing energy conservation. Another time-reversible extrapolation technique is Kolafa's predictor-corrector method [110], which has been proven to yield efficient and energy-conserving algorithms [92] and was introduced simultaneously with the FMD. We note that time-reversible propagators are also extensively used for simulations which do not impose SCF convergence: the requirement is either lifted [94, 92] completely or else relaxed by restricting SCF procedure to several iterations [89] or indeed to a single one [95].

We have seen that use of proper guess-propagation techniques significantly improves com-

putational efficiency and preserves long-term energy conservation. In addition, most such techniques are easy to implement in the programs and are, therefore, highly desirable to be used in BOMD simulations and code development.

5.4 Sampling trajectories

Here we consider only isolated systems in the gas phase: single molecules, clusters or their collisions. Such systems form microcanonical, or NVE, ensembles. Strictly speaking, an isolated molecule is already a microcanonical ensemble. A swarm of such ensembles is characterized by some energy distribution. Trivially, this distribution can be uniform if total energies of all molecules are equal. If they, however, form a Boltzmann distribution, then this set of NVE ensembles mimics canonical (NVT) ensemble of molecules in an ideal gas. In any case, temperature is not present explicitly in the integration but is needed to find total energies used for sampling, that is to final a set of quantum numbers for each of the systems in the swarm. Often temperature is not used at all, for instance, when simulating state-specific or non-equilibrium dynamics.

5.4.1 General theory

To sample a trajectory means to define the initial coordinates and velocities needed as starting conditions to integrate classical equations of motion. Since in the NVE ensemble, the system is not interacting with the surroundings, no equilibration stage is present in the simulations. Therefore, the results of BOMD modeling strongly depend on the quality of the starting conditions. To generate realistic trajectories one needs to have a good approximation to the initial state wave function or its classical analogue [111]. For adiabatic dynamics, complete set of rotational-vibrational wave functions χ_m^n (see Chapter 1) for the selected electronic state n is required. However, accurate solution for the time-independent nuclear problem is as computationally demanding as trajectory simulations. Therefore, a simple "harmonic oscillator-rigid rotor" approximation is routinely used to obtain starting conditions. Then, mixed rotational-vibrational quantum numbers m are split into purely vibrational and rotational numbers N and J.

Analytical solutions of the Schrödinger equation are known as well as expressions for the energy levels:

$$E_{\text{vib}} = (N + \frac{1}{2})\nu, \tag{5.16}$$

$$E_{\text{rot}} = BJ(J+1), \tag{5.17}$$

$$B = \frac{\hbar^2}{2I}, \tag{5.18}$$

where ν is vibrational frequency, B is rotational constant and I is the moment of inertia. There is, of course, $3N-6$ ($3N-5$) vibrational modes, quantum numbers and vibrational frequencies and 3 (2) rotational constants and momenta of inertia for the non-linear (linear) molecule.

Rotational sampling is performed in a trivial manner and we concentrate on sampling vibrations. Generally, the sampling procedure involves the following steps [112, 113].

- Find a stationary point $\mathbf{x}_0$ on the PES, calculate the molecular Hessian, $\mathbf{H}$;
- Solve vibrational problem in the harmonic approximation;
- Sample quantum numbers (vibrational levels and, consequently, energies) according to the assumed energy distribution;
- Sample displacements and momenta (velocities) in normal coordinates;
- Transform displacements and velocities to Cartesian frame, $\Delta\mathbf{x}$ and $\mathbf{v}$, calculate the potential, V^{harm}, and the kinetic energies in harmonic approximation;
- Calculate the electronic energy at $\mathbf{x}_0 + \Delta\mathbf{x}$, V.
- Scale $\Delta\mathbf{x}$ and $\mathbf{v}$ so that $V^{\mathrm{harm}} = V$:

$$\mathbf{x}^{'} = k^{1/2}\mathbf{x}, \tag{5.19}$$

$$\mathbf{v}^{'} = k^{-1/2}\mathbf{v}, \tag{5.20}$$

$$k = \frac{V^{harm}(\Delta\mathbf{x})}{V(\Delta\mathbf{x})}. \tag{5.21}$$

The first two steps are performed once, whereas the others are repeated for each trajectory. Harmonic vibrational problem is solved by the Wilson-Elyashevich method [30, 114] in either Cartesian or internal coordinates [115, 60, 116, 117, 40]. The resulting frequencies are almost identical but using rectilinear and curvilinear normal coordinates may result in quite different finite displacements especially for large-amplitude normal modes [115]. Obviously, those from curvilinear modes are more realistic as discussed in Chapter 4. Quantum numbers are selected manually or found by any procedure such as the von Neumann rejection technique [118] based on the value of the total energy or the temperature.

Subsequently, displacements and velocities may be sampled either in a classical [112, 113] or in a quantum [113] manner using Wigner [119] Husimi [120, 121] functions. In the application that follows, we sample Boltzmann distribution for each mode at a certain temperature and the find canonical coordinates and momenta for the ith mode classically as follows:

$$Q_i = (2E_i/f_i)^{1/2}\cos 2\Pi R_i, \tag{5.22}$$

$$P_i = (2E_i)^{1/2}\sin 2\Pi R_i, \tag{5.23}$$

In these equations, E_i is the energy of the harmonic vibration in the selected state, f_i is the corresponding vibrational eigenvalue, and R_i is a newly generated random number uniformly distributed in $[0; 1]$ range.

Next, the sampled displacements are transformed into the Cartesian frame. For rectilinear normal modes, this transformation is linear, whereas for curvilinear normal modes it was discussed in Chapter 4. If the HOPE back-transformation is applied, then for all the ensemble only one matrix inverse is needed and the procedure will not add computational effort beyond the sampling in Cartesian coordinates.

Table 5.1: Sampling of acetone at 300, 500 and 700 K using rectilinear and curvilinear normal coordinates at DFT/BLYP/6-311G** level of theory.

	Mean error, a.u.		maximal error, a.u.		Mean deviation of k from 1.0		average k	
	rect.	curv.	rect.	curv.	rect.	curv.	rect.	curv.
300 K	0.032	0.013	0.220	0.053	0.245	0.135	0.774	0.920
500 K	0.032	0.013	0.168	0.036	0.241	0.126	0.789	0.939
700 K	0.035	0.013	0.410	0.052	0.248	0.130	0.777	0.927

The scaling in the final step is meant to introduce the corrections for anharmonicity, which inevitably arises for finite displacements from the stationary point [122]. Although this procedure gives the correct energy (macrostate), it distorts the microstate since coordinates are scaled uniformly although their contributions to anharmonicity are different.

5.4.2 Performance of sampling in Cartesian and internal coordinates

We have tested sampling in Cartesian and curvilinear normal modes on the acetone molecule $CH_3 - CO - CH_3$ at DFT/BLYP/6-311G** level of electronic structure theory (see paper V). We have sampled three sets of 300 trajectories, each from a Boltzmann distribution at three termeratures: 300 K, 500 K and 700 K. To facilitate comparison we used the same vibrational quantum numbers and random phases in eqs. (5.22) for the curvilinear and rectilinear-mode samplings. The results are given in Table 5.1.

It is readily seen that the use of curvilinear normal coordinates reduces both accumulated and maximal error in the potential energy substantially. The RMS deviation of the scaling coefficient is also reduced by about a factor of two. Thus, the use of curvilinear normal modes significantly improves the quality of the sampling in a simple black-box fashion, requiring almost no additional computational effort provided the HOPE internal-to-Cartesian back transformation is utilized.

5.5 BOMD and observable quantities

Classical equations of motion in BOMD approximate nuclear Schrödinger equation. Besides, classical trajectories can form distinct ensembles. Therefore, it is in principle possible to calculate any observable quantity, either time dependent or not, based on BOMD. These quantities are not restricted to quantum-mechanical observables but include thermodynamical functions [99], rate coefficients [31], mass-spectra [123], kinetic energy release [62] and other measurable properties.

As far as the latter are concerned, from classical statistical physics we know that phase-space information is enough to calculate thermodynamic observables by utilizing ergodicity, provided a proper ensemble has been modelled [99]. If time-averaging is not performed, then time-resolved properties can be evaluated. Counting the outcomes of the reactive trajectories gives branching ratios, selectivities as well as mass-spectra in a special case of fragmentation after ionization. The time distribution of reactive events gives rate coefficients.

To obtain quantum-mechanical observables from BOMD trajectories, there are two main

approaches. The first one is again averaging: a property is computed along the trajectory either at each time step or at selected geometries sampled during the integration before averaging. Examples are NMR chemical shifts [124] and thermally-averaged molecular structure [125].

Other properties can be computed by Fourier transformation of autocorrelation functions. Hence, the infrared spectrum [126] – intensity I vs. frequency ω – can be calculated as follows:

$$I(\omega) = \propto \int_0^\infty \langle \mu(t) \cdot \mu(0) \rangle \, cos(\omega t) dt, \tag{5.24}$$

where $\mu(t)$, $\mu(0)$ are electronic dipole moments corresponding to nuclei configuration at time t and in the beginning of the trajectory, whereas $\langle \mu(t) \cdot \mu(0) \rangle$ is the autocorrelation function. Eq. (5.24) is nothing but a linear response equation. Raman spectra are obtained analogously, using the polarizability autocorrelation function [127].

These techniques for obtaining observables combined with efficient integration algorithms combine to make BOMD a popular and powerful tool for chemistry and physics.

5.6 Accuracy of BOMD calculations

To conclude the discussion of BOMD, we must consider the accuracy of such simulations. Unfortunately, it is difficult to assess the accuracy of BOMD since it is an intrinsically composite method. Indeed, there are at least six major sources of errors:

- the Born-Oppenheimer approximation;
- neglect of quantum effects on the motion of the nuclei;
- deficiencies of the selected electronic structure theory level;
- mechanical errors inherent in the integration algorithm;
- an incomplete statistical description;
- drawbacks of the method used to extract observables from trajectories.

All these issues have been discussed above. In reality, errors from different sources may either add up or cancel giving "the right answer for the wrong reason". Each case is individual and all the constituents of a BOMD calculation should be carefully selected. In general, BOMD is believed to give reliable qualitative and semi-quantitative results, although a significant number of the approximations involved seldom allow obtaining results of excellent qualitative precision [88, 64]. One of the reasons is the fact that most applications are performed at quite low levels of electronic structure theory, electronic structure calculations being the bottleneck in the simulations. Further advances in reducing the scaling of accurate methods must improve on the precision of observable quantities calculated by BOMD.

Chapter 6

Implementation of PES exploration algorithms

A number of algorithms for PES exploration has been implemented in the Dalton2013 quantum chemistry program suite [128], a powerful tool for electronic structure and molecular properties calculations at HF, DFT, MCSCF, CC levels of theory (see paper III). The kernel of the suite are two programs Dalton and LSDALTON. The former has a longer history (since 1983) and, consequently, provides a wider choice of *ab initio* and DFT electronic structure methods as well as molecular properties than the latter. The LSDALTON project was started in 2006, primarily to create a linear-scaling implementation of DFT. This goal has been to a large extent fulfilled. In addition, LSDALTON has functionality for linear-scaling MP2 and CCSD calculations.

For the most part, Dalton2013 is written in Fortran: Dalton – in Fortran 77, while LSDALTON – in Fortran 90. Both programs contain some C code. In addition, LSDALTON utilizes C++. Both programs work on most Unix-based operational systems. Some important computationally expensive parts of the codes are parallelized using MPI (distributed memory systems) in Dalton and a hybrid OpenMP/MPI (distributed memory/shared memory systems) in LSDALTON. Dalton is distributed as source code free of charge [128].

The author of this thesis has contributed mostly to the linear-scaling LSDALTON program, having created modules for BOMD, geometry optimization and coordinate transformations. The optimization module of LSDALTON is essentially the original Dalton optimizer rewritten from Fortran 77 to Fortran 90, while the modules for BOMD and internal-to-Cartesian step back transformation have been created anew.

All optimization algorithms implemented in LSDALTON are based on the trust-radius quasi-Newton method in either Cartesian, or internal coordinates [67]. The initial approximate Hessian may be a unit matrix, or a matrix based on a primitive diagonal force field model (0.5 for bonds, 0.2 for angles and 0.1 for dihedrals) and a more refined diagonal model [132]. A variety of Hessian update schemes are available: Powell-symmetric-Broyden, Davidson-Fletcher-Powell, Broyden-Fletcher-Shanno-Goldfarb [133] and Bofill's formula [134]. The code is able to locate both PES minima and TS. Two sets of criteria to check optimization convergence are utilized. The first is more suitable for smaller molecules [135] and is based on the threshold for the maximum absolute element of the molecular gradient and for the step components, or the change of the energy from the previous iteration. The other set of criteria is more suitable for optimizations of large systems and includes the root-mean-square of the gradient, its maximum

absolute element, the root-mean-square of the step vector, and its maximum absolute element in internal coordinates [136].

The module for internal-to-Cartesian geometric step transformation includes the IBT, SIBT and HOPE schemes. Derivatives of internal coordinates, required for the HOPE method, are evaluated by means of automatic differentiation using lybtaylor library written by Ekström in C++. If the back-transformation fails to converge the step, then the linearized estimate is accepted.

A gradient-based velocity-Verlet integrator in Cartesian coordinates for a microcanonical ensemble is the basis for the BOMD module. Trajectories can be integrated at all electronic structure levels available in LSDALTON. Fock matrix dynamics and the time-reversible filter guess propagators are implemented in the code and can be used at the HF and DFT levels. It is also possible to calculate all available molecular properties along the trajectories. In addition, canonical ensembles can be modelled by applying the Nose-Hoover chain thermostat, the implementation being based on explicit reversible integrators [131]. The mechanical accuracy of integration can be estimated from energy drift and energy noise, which are calculated at the end of each trajectory. The scheme for sampling microcanonical ensembles in curvilinear internal coordinates is implemented in a Python script. The script reads in the analytical Hessian and internal coordinates determined by Dalton as input. It also employs libtaylor [137] for performing the HOPE back transformation.

To model mechanochemical processes, the EFEI model of external force is implemented. It is available for both BOMD and geometry optimizations. Currently, it allows application of force to any singe pair of atoms in the molecule.

In addition, a suit of Python scripts has been developed for analyzing trajectories integrated with LSDALTON: to extract .xyz files for visualization with VMD [138]; to calculate IR-spectra, kinetic energy release, unimolecular dissociation rate coefficients; to detect structural rearrangements in water clusters.

The developments and implementations described above combine to make LSDALTON a powerful tool for large-scale MD simulations of unimolecular reactions using electronic structure theory.

Chapter 7

Applications

Most of the calculations reported here have been performed using LSDALTON and Python script suite. Although the chemistry of water clusters and the mechanochemistry of alkanes represent different branches of the chemical science, these particular studies are united by a common methodology: PES exploration, mainly by BOMD. Hence, they may serve to illustrate how established theoretical concepts, efficiently implemented in a computer code, can be useful for wide areas of modern molecular science.

7.1 Protonated water clusters

Protonated water clusters exhibit strong dependence of intensity in mass-spectra on cluster size [139]. Several $(H_2O)_nH^+$ electrospray-generated ions are much more intensive than those with neighbouring n. Such clusters occur at *magic number*, the smallest magic number being $n = 21$. The abnormal intensity of these clusters in mass-spectra is generally attributed to higher stability of particular species. We have performed BOMD simulations with an aim to explain the nature of magic-number clusters by comparing one of these, $(H_2O)_{21}H^+$, with an "ordinary" $(H_2O)_{20}H^+$ cluster. The specific objectives of the study were to reveal dynamical geometric structures, to find evaporation rate and mechanisms and to study proton transfer processes.

All calculations were carried out at the DFT/BLYP/6-31G+(d,p) level of electronic structure theory, with and without an empirical dispersion correction [140]. Trajectories were quasiclassically sampled as NVE ensembles corresponding to a temperature of 200 K and integrated for 2.5 ps. The total number of trajectories is 80. More computational details are given in Paper I. It was immediately observed that the absence of a dispersion correction leads to unreasonably fast water evaporation. Therefore, only the results for the dispersion-corrected calculations are discussed hereafter.

7.1.1 Geometrical structure and relative stability

Using high-level *ab initio* data [84] and our own preliminary DFT calculations to initialize trajectories, we have selected the two energetically most favourable isomers for $n = 20$ and $n = 21$: cage and dodecahedron (see Fig. 7.1 and 7.2).

Surprisingly, evaporation rate and proton transfer for the two sizes and the two shapes were found to be very similar, not exhibiting any explicit size- and shape-dependences. Thus, the

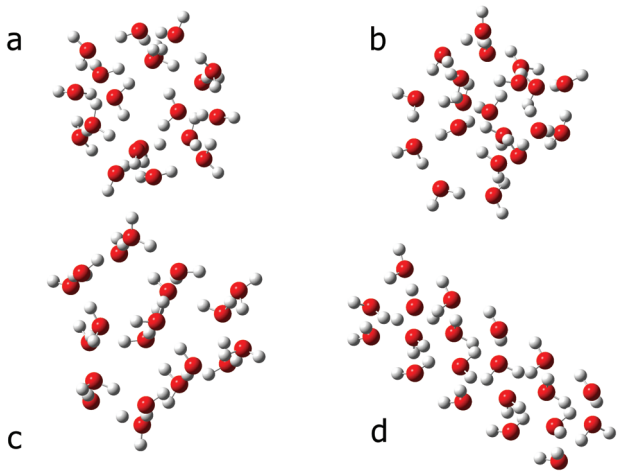

Figure 7.1: Structures of the $(H_2O)_{20}H^+$ clusters optimized at the BLYP/6-31+G(d,p) level: a) dodecahedron, b) cage, c) prismic, and d) cubic.

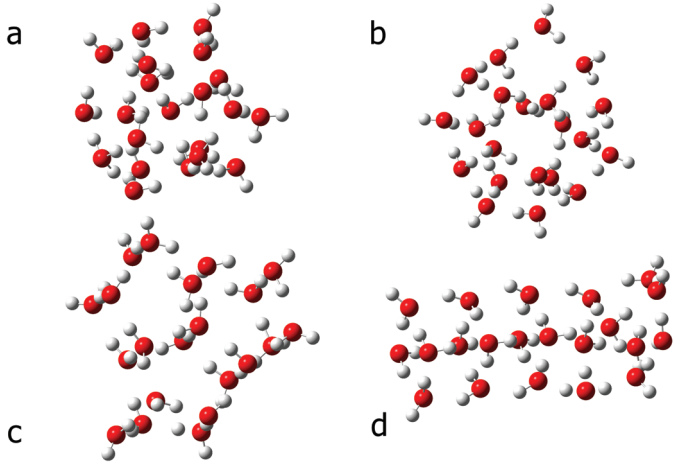

Figure 7.2: Structures of the $(H_2O)_{21}H^+$ clusters optimized at the BLYP/6-31+G(d,p) level: a) dodecahedron, b) cage, c) prismic, and d) cubic.

magic-number problem was left unsolved. Nevertheless, much useful information about evaporation and proton transfer was obtained, no dramatic differences between clusters of different sizes and shapes being observed.

7.1.2 Evaporation mechanisms and kinetics

Three mechanisms for cluster evaporation were revealed (see Fig. 7.3): loss of a single water molecule (about one quarter of the dissociation events), sequential loss of several water molecules (about one quarter of the dissociation events) and losing water dimers and overall "loosening" of the cluster (about one half of the dissociation events). The apparent dissociation rate coefficient was estimated to be of the order of $10^{11}\ \mathrm{s}^{-1}$. The values of kinetic energy release after the dissociation show that the evaporated molecules acquire on average thermal energy corresponding to 200 K. Consequently, evaporation does not lead to "cooling" of the clusters.

7.1.3 Proton transfer

The Grotthus chain mechanism in protonated water clusters closely resembles that in bulk water [141]. Indeed, what occurs is not a proton transfer but rather a transfer of the solvation shell to a neighbouring location (see Fig. 7.4). The solvation shell is a mixture of the Eigen and Zundel structural motifs. In the former, $(\mathrm{H_2O})_3\mathrm{H}^+$, there are three equivalent protons connecting the central oxygen atom with the three water fragments. In the latter, $(\mathrm{H_2O})_2\mathrm{H}^+$, there is only one between the two water fragments. As for the clusters, there are two equivalent protons - H(1) and H(2) in Fig. 7.4, while a third proton, H(3), is situated further away from the central proton in the solvation shell.

Unlike in bulk water, there are freely dangling $\mathrm{O}-\mathrm{H}$ bonds (i.e. not hydrogen-bonded). We observed in the simulations that proton transfer often leads to the hydrogen-bond network rearrangement, increasing the number of dangling bonds and reducing the number of the hydrogen-bonded ones. Thus, in clusters, proton transfer can facilitate dissociation.

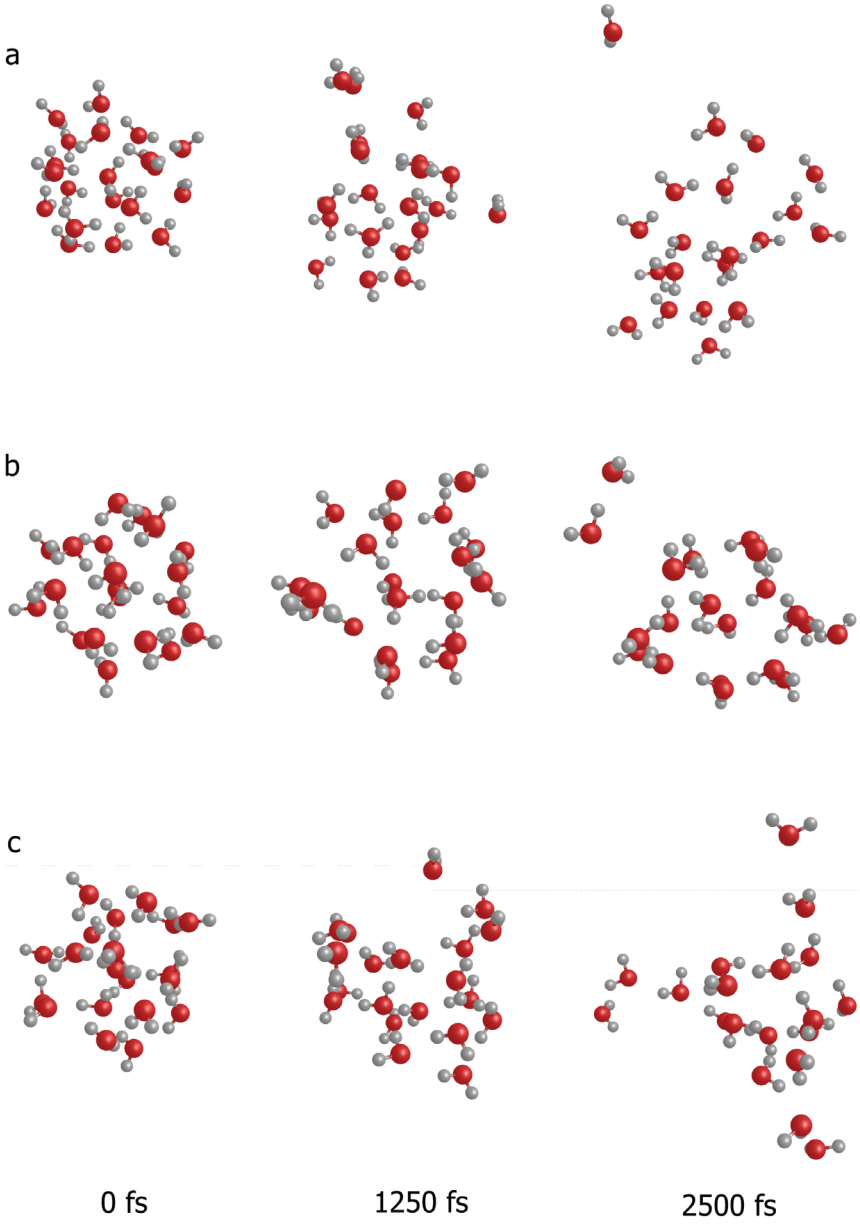

Figure 7.3: Prototypical trajectories for $(H_2O)_nH^+$ clusters calculated at the BLYP-D/6-31+G(d,p) level (illustrated by$(H_2O)_{21}H^+$ trajectories with the initial configuration of the cage): a) single water molecule elimination, b) loss of several water molecules, and c) "loosening" of the cluster.

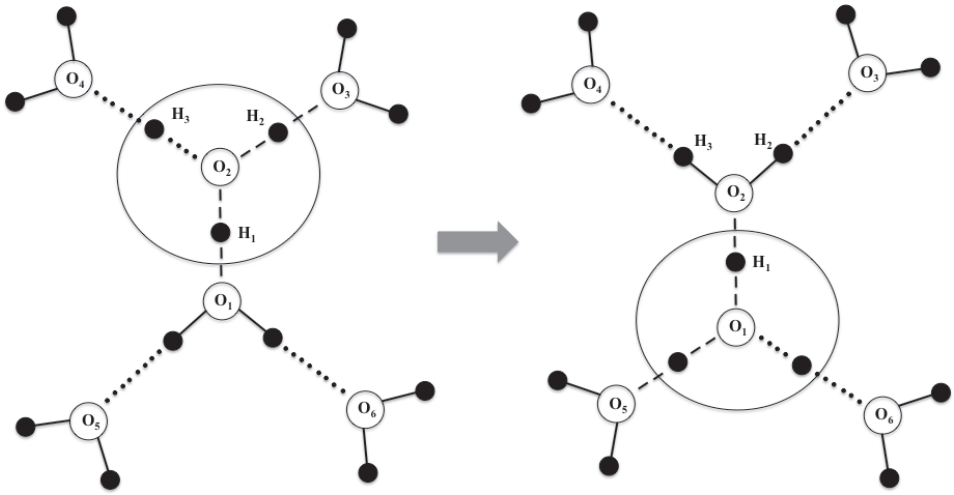

Figure 7.4: Example of a proton transfer event leading to the destruction of one solvation shell through the formation of another.

7.2 Mechanochemistry of n-alkanes

Linear alkanes are prototypes of polymers. Indeed, from a chemical point of view, polyethylene is nothing but a very long alkane chain,mostly, linear. Understanding the effect of the external force on n-alkanes will shed light on mechanochemistry of polymers [142]. In addition, simple chain molecules are ideal models for understanding the general role of dynamics in mechanical activation.

We have studied n-butane and n-octane with the pulling external force acting on the terminal carbon atoms using the EFEI model. Two prototypical scenarios were considered:

- **Fixed-force scenario:** The molecule is first prepared in the equilibrium configuration corresponding to an externally applied fixed force, a thermodynamically equilibrated ensemble is created, and the dynamics is run under the constraint of the fixed force.

- **Sudden-force scenario:** The molecule is prepared in a thermodynamically equilibrated ensemble at the equilibrium geometry in the absence of an external force, and the dynamics is run with a suddenly applied force.

The first case represents a process where the molecule is stretched gradually and kept close to thermodynamical equilibrium during the stretching. This scenario mimics the atomic-force microscopy experiments on molecule stretching called *single-molecule force spectroscopy* [143]. In the second case, the molecule is subject to forces induced in the medium by ultrasound action [144].

The forces were selected close to the critical rupture force of a $\mathrm{C}-\mathrm{C}$ bond. This ensures non-applicability of the Bell's theory. We performed BOMD simulations (a total of 420 trajectories of 2 ps duration) quasiclassically sampled as NVE ensembles corresponding to 300 K. In addition, TST calculations for a single terminal $\mathrm{C}-\mathrm{C}$ bond dissociation in the fixed-force scenario were carried out. The electronic structure theory level was DFT/B3LYP/6-311+G**. More details are given in Paper IV.

7.2.1 Fixed-force simulations

Three main outcomes of the trajectories were revealed: the breaking of a single terminal $\mathrm{C}-\mathrm{C}$ bond, the breaking of both terminal bonds simultaneously, and the breaking of both terminal bonds consecutively (see Fig. 7.5).

The ratio of these mechanisms depends on the force magnitude, but in general shifts from one bond rupture to multiple bond ruptures with its increase. The subsequent mechanism is the result of a two step process where, as soon as one bond is broken, the external force pulls the fragments apart and a shock wave arises in the larger fragment. In many instances, the travelling shock wave induces a second bond breaking event shortly after. In Fig. 7.6, the delay time divided by the separation between the ruptured bonds is plotted for the force value for which double rupture is most frequent. For butane, the distribution is centred around 10 km/s, which corresponds to the speed of the shock wave (similar to the speed of sound in light solids). For octane, no peak is observed, suggesting that the shock-wave mechanism is unimportant for this molecule at a high force.

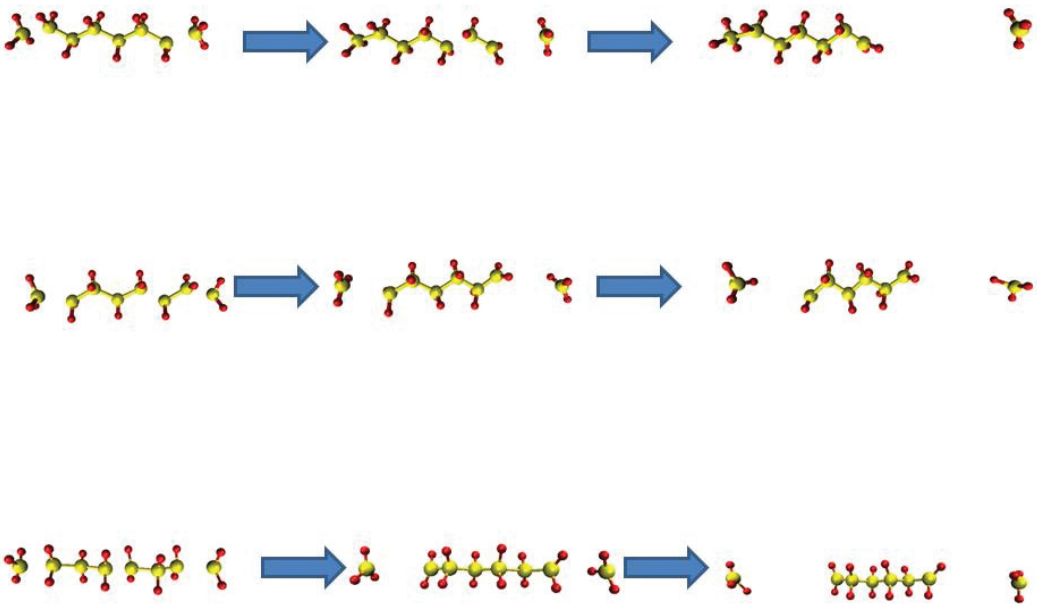

Figure 7.5: Bond breaking mechanisms: a - single bond breaking, b - breaking of both terminal bonds with delay, c - simultaneous breaking of both terminal bonds.

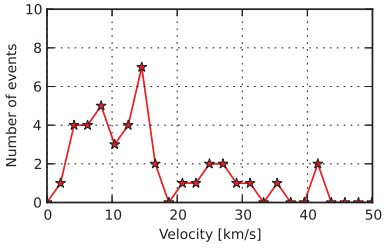

(a) butane, $F^{supercrit}$, 300 K

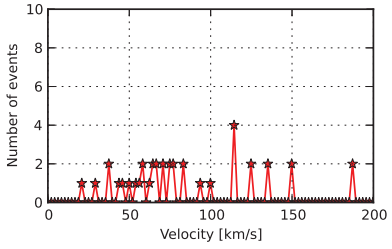

(b) octane, $F^{supercrit}$, 300 K

Figure 7.6: Distribution of time between the first and second bond breakage divided by distance between the two bonds broken. The peaks at 10km/s represents the speed of a shock wave.

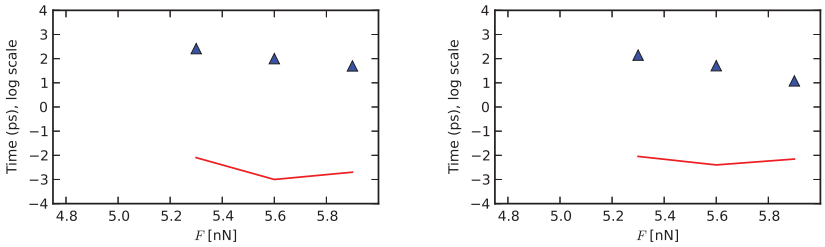

(a) Butane, 300 K

(b) Octane, 300 K

Figure 7.7: Bond breaking time as a function of force, − TST, , △ BOMD.

7.2.2 Sudden force simulations

In the sudden force scenario, the results of the simulations are quite different from those in the fixed-force scenario. In particular, the magnitude of the external force able to break a bond is significantly reduced. Besides, a greater variety of bond-breaking mechanisms is observed: also bonds in the middle of the chain are being broken.

7.2.3 BOMD vs. TST

BOMD and TST rates were compared only for the fixed-force simulations. We assumed that simultaneous terminal bond breaking mechanism does not have significant effect on the kinetics in the frame of TST, since the corresponding activation barrier must be much higher than the one to break a single bond. Apparent bond breaking times are plotted in Fig. 7.7. The rates obtained from BOMD are significantly lower than those from TST. In fact, TST predicts almost immediate bond dissociation, which does not appear physical.

This behaviour can be rationalized bearing in mind that TST assumes immediate energy randomization, while BOMD incorporates an induction period. It provide sufficient time for energy redistribution, leading to a situation where bond breaking may occur. This makes the details of the vibrational pattern important. In particular, the phases of low-frequency stretch modes play a crucial role for short-time chain stability. Thus, antiphase motion enhances the mechanochemical strength, while supplying energy to low-frequency symmetric stretch facilitates the dissociation.

Conclusions

We started the thesis with the consideration of the Born-Oppenheimer approximation. This separation of variables in the molecular Schrödinger equation leads to far-reaching consequences. Indeed, the splitting of the molecular problem into the electronic and the nuclear ones lays down the foundations of theoretical chemistry, from both conceptual and computational points of view. The most important concept for the thesis is the potential energy surface (PES), obtained by electronic structure methods and defining the dynamics of the nuclei. The latter was in the focus of this work.

A number of further approximations beyond the Born-Oppenheimer approximation give rise to practical methods for studying molecular properties, structure and reaction dynamics. One such approach is Born-Oppenheimer molecular dynamics (BOMD), treating the nuclei as classical particles, moving on the PES obtained by electronic structure calculations. For this thesis, a new module for BOMD simulations in the Dalton program suite has been created, incorporating modern achievements of the trajectory integration techniques and the advances in electronic structure methods.

Another important topic in this work was coordinate systems and transformations. A proper selection of the coordinate system significantly facilitates PES exploration, provided the necessary transformations to and from this coordinate system are accurate and computationally cheap. It turns out that chemically motivated curvilinear internal coordinates are well-suited for many theoretical techniques. However, their use gives rise to an internal-to-Cartesian back transformation problem, which does not have an exact analytical solution. The required transformations can be computationally expensive and numerically unreliable. In this work, we have proposed the high-order path-expansion (HOPE) back transformation, which has proved to be robust and efficient. We have also found another application for curvilinear internal coordinates: for sampling the initial conditions of the trajectories in the harmonic approximation. A simple black-box technique significantly improves the quality of the sampling.

Finally, the methods and the code developed presented in this thesis were used to study the dynamics of "real-world" chemical systems: protonated water clusters and alkanes under mechanical stress. The former study is relevant for atmospheric chemistry, whereas the latter concerns the behaviour of polymers under mechanical stress, comparing dynamical and statistical descriptions. In both cases, a detailed mechanistic picture of dissociation has been obtained and the unimolecular rate coefficients have been calculated.

Hence, we have gone the whole way from the basic foundations of molecular dynamics to the important chemical applications via extensive method and code developments. The theoretical tools created are sufficiently efficient and general to be applicable to a wide range of chemical systems and problems. Importantly, the developed code has been made accessible to

the chemical community through the distribution of the Dalton package, free of charge.

Bibliography

[1] P. Jensen and P. R. Bunker, in *Computational Molecular Spectroscopy*, edited by P. Jensen and P. R. Bunker (John Wiley & Sons, Chichester, 2000).

[2] M. Born and K. Huang, *Dynamical Theory of Crystal Lattices* (Oxford University Press, Oxford, 1954).

[3] P. R. Bunker, C. J. McLarnon, and R. E. Moss, Mol. Phys. **33**, 425 (1977).

[4] I. Mayer, *Simple Theorems, Proofs and Derivations in Quantum Chemistry* (Kluwer Academic/Plenum Publishers, New York, 2003).

[5] M. Born and R. Oppenheimer, Annalen der Physik **389**, 457 (1927).

[6] P. Atkins and R. Friedman, *Molecular Quantum Mechanics, Fifth Edition* (Oxford University Press, Oxford, 2010).

[7] K. Gavroglu and A. Simoes, *Neither Physics, nor Chemistry: a History of Quantum Chemistry* (MIT Press, Cambridge MA, London, 2012).

[8] W. Heitler and F. London, Zeitschrifr für Physik **44**, 455 (1927).

[9] T. Helgaker, P. Jørgensen, and J. Olsen, *Molecular Electronic-Structure Theory* (John Wiley & Sons, Chichester, 2000).

[10] C. Hättig, W. Klopper, and A. Köhn, and D. P. Tew, Chem. Rev. **112**, 4 (2012).

[11] P. Hohenberg and W. Kohn, Phys. Rev. **136**, B864 (1964).

[12] E. H. Lieb, Phys. Rev. Lett. **46**, 457 (1981).

[13] W. Kohn and L. J. Sham, Phys. Rev. **140**, A1133 (1965).

[14] R. G. Parr and W. Yang (1994), *Density-Functional Theory of Atoms and Molecules* (Oxford University Press, Oxford, 1994).

[15] A. D. Becke, Phys. Rev. A **38**, 3098 (1988).

[16] A. D. Becke, J. Chem. Phys. **98**, 1372 (1993).

[17] E. Runge and E. K. U. Gross, Phys. Rev. Lett. **52**, 997 (1984).

[18] M. J. G. Peach, P. Benfield, T. Helgaker, and D. J. Tozer, J. Chem. Phys. **128**, 044118 (2008).

[19] E. E. Dahlke, R. M. Olson, H. R. Leverentz, and D. G. Truhlar, J. Phys. Chem. A **112**, 3976 (2008).

[20] S. Reine, T. Helgaker, and R. Lindh, WIRES: Comput. Mol. Sci. **2**, 290 (2012).

[21] P. Pulay, Mol. Phys. **17**, 197 (1969).

[22] F. B. van Duijneveldt, J. G. C. M. van Duijneveldt - van de Rijdt, and J. H. van Lenthe, Chem. Rev. **1994**, 1873 (1994).

[23] L. Genovese, A, Neelov, S. Goedecker, T. Deutsch, S. A. Ghasemi, A. Willand, D. Caliste, O. Zilberberg, O. Rayson, A. Bergman, and R. Schneider, J. Chem. Phys. **129**, 014109 (2008).

[24] L. Frediani, E. Fossgaard, T. Flå, and K. Ruud, Mol. Phys. **111**, 1143 (2013).

[25] R. J. Harrison, G. I. Fann, T. Yanai, Z. Gan, and G. Beylkin, J. Chem. Phys. **121**, 11587 (2004).

[26] F. A. Bischoff and E. F. Valeev, J. Chem. Phys. **2013**, 114106 (2013).

[27] T. Helgaker, P. Jørgensen, and N. C. Handy, Theor. Chem. Acc. **76**, 227 (1989).

[28] P. Jørgensen and J. Simons, J. Chem. Phys. **79**, 334 (1983).

[29] C. Eckart, Phys. Rev. **47**, 552 (1935).

[30] E. B. Wilson Jr., J. C. Decius, and P. C. Cross, *Molecular Vibrations—The Theory of Infrared and Raman Vibrational Spectra* (Dover, New York, 1980).

[31] A. Fernandez-Ramos, J. A. Miller, S. J. Klippenstein, and D. G. Truhlar, Chem. Rev. **106**, 4518 (2006).

[32] K. Fukui, Acc. Chem. Res. **14**, 363 (1981).

[33] P. L. Houston, *Chemical Kinetics and Reaction Dynamics* (McGraw-Hill, New York, 2001).

[34] L. Landau and E. Lifshitz, *Mechanics* (Pergamon Press, Oxford, 1960).

[35] N. A. Smirnova, *Methods of Statistical Thermodynamics in Physical Chemistry* (Vysshaya Shkola, Moscow, 1982), in Russian.

[36] D. Marx and J. Hutter, *Ab Initio Molecular Dynamics: Basic Theory and Advanced Methods* (Cambridge University Press, Cambridge, 2009).

[37] D. Marx and M. Parrinello, J. Chem. Phys. **104**, 4077 (1996).

[38] N. Makri and W. H. Miller, J. Chem. Phys. **91**, 4026 (1989).

[39] J. Kästner, WIRES: Comput. Mol. Sci. DOI: 10.1002/wcms.1165 (2013).

[40] F. Jensen, *Introduction to Computational Chemistry* (John Wiley & Sons, Chichester, 2006).

[41] H. M. Senn and W. Thiel, Angew. Chem. Int. Ed. **48**, 1198 (2009).

[42] A. S. Sanz, X. Gimenez, J. M. Bofill, and S. Miret-Artes, Chem. Phys. Lett. **478**, 89 (2009).

[43] D. Bohm, Phys. Rev. **85**, 166 (1952).

[44] S. L. James and T. Friscic, Chem. Soc. Rev. **42**, 7494 (2013).

[45] K. Wolinski and J. Baker, Mol. Phys. **108**, 1845 (2010).

[46] M. Grandbois, M. Beyer, M. Rief, H. Clausen-Shaumann, and H. E. Graub, Science **283**, 1727 (1999).

[47] M. T. Ong, J. Leiding, H. Tau, A. M. Virshup, and T. J. Martinez, J. Am. Chem. Soc. **131**, 6377 (2009).

[48] J. Ribas-Arino, M. Shiga, and D. Marx, Angew. Chem. Int. Ed. **48**, 4190 (2009).

[49] G. I. Bell, Science **200**, 618 (1978).

[50] S. S. M. Konda, J. N. Brantley, C. W. Bielawski, and D. E. Makarov, J. Chem. Phys. **135**, 164103 (2011).

[51] P. Dopieralski, J. Ribas-Arino, P. Anjukandi, M. Krupicka, J. Kiss, and D. Marx, Nat. Chem. **5**, 685 (2013).

[52] L. D. Landau and E. M. Lifshitz, *Statistical Physics* (Pergamon Press, Oxford, 1969).

[53] J. Baker, J. Comput. Chem. **13**, 240 (1992).

[54] J. P. Ryckaert, G. Ciccotti, and H. J. C. Berendsen, J. Comput. Phys. **23**, 327 (1997).

[55] P. Schmelcher and L.S. Cederbaum, Int. J. Quant. Chem. **S25**, 371 (1991).

[56] H. B. Schlegel, WIRES: Comput. Mol. Sci. **112**, 790 (2011).

[57] H. B. Schlegel, J. Comput. Chem. **24**, 1514 (2003).

[58] S. K. Burger and P. W. Ayers, J. Chem. Phys. **132**, 234110 (2010).

[59] J. M. Bofill and J. M. Anglada, Theor. Chem. Acc. **105**, 463 (2001).

[60] H. Dachsel, D. Sosna, and W. Quapp, J. Mol. Struct (Theochem) **315**, 315 (1994).

[61] F. Jensen and D. S. Palmer, J. Chem. Theory Comput. **7**, 223 (2011).

[62] T. Helgaker, E. Uggerud, and H. J. Aa. Jensen, Chem. Phys. Lett. **173**, 145 (1990).

[63] J. M. Millam, V. Bakken, W. Chen, W. L. Hase, and H. B. Schlegel, J. Chem. Phys. **111**, 3800 (1999).

[64] U. Lourderaj, K. Song, T. L. Windus, Y. Zhuang, and W. L. Hase, J. Chem. Phys. **126**, 044105 (2007).

[65] A. K. Mazur, V. E. Dorofeev, and R. A. Abagyan, J. Comput. Phys. **92**, 261 (1991).

[66] P. Pulay and B. Paizs, Chem. Phys. Lett. **353**, 400 (2002).

[67] V. Bakken and T. Helgaker, J. Chem. Phys., **117**, 9160 (2002).

[68] T. Jordan, *Linear Operators for Quantum Mechanics* (John Wiley & Sons, New York, 1969).

[69] C. Peng, P. Y. Ayala, H. B. Schlegel, and M. J. Frisch, J. Comput. Chem. **17**, 49 (1996).

[70] M. von Arnim and R. Ahlrichs, J. Chem. Phys. **111**, 9183 (1999).

[71] S. R. Billeter, A. J. Turner, and W. Thiel, Phys. Chem. Chem. Phys. **2**, 2177 (2000).

[72] J. C. Decius, J. Chem. Phys. **17**, 1315 (1949).

[73] P. Pulay, G. Fogarasi, F. Pang, and J. E. Boggs, J. Am. Chem. Soc. **101**, 2550 (1979).

[74] K. Nemeth and M. Challacombe, J. Chem. Phys. **121**, 2877 (2004).

[75] J. Andzelm, R. D. King-Smith, and G. Fitzgerald, Chem. Phys. Lett. **335**, 321 (2001).

[76] J. Baker, A. Kessi, and B. Delley, J. Chem. Phys. **105**, 192 (1996).

[77] J. Baker and W. J. Hehre, J. Comput. Chem. **12**, 606 (1991).

[78] M. A. Collins and D. F. Parsons, J. Chem. Phys. **99**, 6754 (1993).

[79] E. F. Koslover and D. J. Wales, J. Chem. Phys. **127**, 234105 (2007).

[80] M. Carlsen, J. Comput. Chem. **35**, 1149 (2014).

[81] J. Baker, D. Kinghorn, and P. Pulay, J. Chem. Phys. **110**, 4991 (1999).

[82] K. Nemeth, M. Challacombe, and M. Van Veenendaal, J. Comput. Chem. **31**, 2078 (2010).

[83] J. L. Wang, X. L. Zhou, G. H. Wang, G. H., and J. J. Zhao, Phys. Rev. B, 71, 113412 (2005).

[84] T. Kus, V. F. Lotrich, A. Perera, and R. J. Bartlett, J. Chem. Phys., **131**, 104313 (2009).

[85] K. Kurotobi and Y. Murata, Science, **333**, 613 (2011).

[86] M. J. Ryding, A. S. Zatula, P. U. Andersson, and E. Uggerud, Phys. Chem. Chem. Phys., **13**, 13, 1356 (2011).

[87] A. Griewank and A. Walther, *Evaluating Derivatives: Principles and Techniques of Algorithmic Differentiation, Second Edition* (SIAM, Philadelphia, PA, 2008; Other Titles in Applied Mathematics 105).

[88] A. Gonzalez-Lafont, T.N. Truong, and D.G. Truhlar, J. Chem. Phys. **95**, 4618 (1991).

[89] A.M.N. Niklasson, Phys. Rev. Lett. **100**, 123004 (2008).

[90] J. Hutter, WIRES: Comput. Mol. Sci. **2**, 604 (2012).

[91] R. Car and M. Parrinello, Phys. Rev. Lett. **55**, 2471 (1985).

[92] T. D. Kühne, M. Krack, F. R. Mohamed, and M. Parrinello, Phys. Rev. Lett. **98**, 066401 (2007).

[93] T. D. Kühne, WIRES: Comput. Mol. Sci. DOI: 10.1002/WCMS.1176 (2013).

[94] A. M. N. Niklasson and M. J. Cawkwell, Phys. Rev. B **86**, 174308 (2012).

[95] P. Souvatzis and A. M. N. Niklasson, J. Chem. Phys. **139**, 214102 (2013).

[96] P. Souvatzis and A. M. N. Niklasson, J. Chem. Phys. **140**, 044117 (2014).

[97] C. Leforestier, J. Chem. Phys. **68**, 4406 (1978).

[98] W. H. Press, S. A. Teukolsky, W. T. Vetterling, and B. P. Flannery, *Numerical Recipes, Third Edition: the Art of Parallel Scientific Computing* (Cambridge University Press, Cambridge, 2007).

[99] D. Frenkel and B. Smit, *Understanding Molecular Simulation, Second Edition: From Algorithms to Applications* (Academic Press, London, 2002).

[100] L. Verlet, Phys. Rev. **159**, 98 (1967).

[101] A. Odell, A. Delin, B. Johansson, N. Back, M. Challacombe, and A.M.N. Niklasson, J. Chem. Phys. **131**, 244106 (2009).

[102] V. Bakken, J. M. Millam, and H. B. Schlegel, J. Chem. Phys. **111**, 8773 (1999).

[103] S. K. Gray, D. W. Noid, and B. G. Sumpter, J. Chem. Phys. **101**, 4062 (1994).

[104] M. Head-Gordon and J. A. Pople, J. Phys. Chem. **92**, 3063 (1988).

[105] P. Pulay and G. Fogarasi, Chem. Phys. Lett. **386**, 272 (2004).

[106] J. M. Herbert and M. Head-Gordon, Chem. Phys. Phys. Chem. **7**, 3269 (2005).

[107] A. M. N. Niklasson, C. J. Tymczak, and M. Challacombe, Phys. Rev. Lett. **97**, 123001 (2006).

[108] A. M. N. Niklasson, P. Steneteg, A. Odell, N. Bock, M. Challacombe, C. J. Tymczak, E. Holmstrøm, G. S. Zheng, and V. Weber, J. Chem. Phys. **130**, 214109 (2009).

[109] G. S. Zhang, A. M. N. Niklasson, and M. Karplus, J. Chem. Phys. **135**, 044122 (2011).

[110] J. Kolafa, J. Comput. Chem. **25**, 335 (2004).

[111] P. Manikandan and W.L.Hase, J. Chem. Phys. **1362**, 184110 (2012).

[112] W.L. Hase and D. G. Buckowski, Chem. Phys. Lett. **74**, 284 (1980).

[113] K. Park, J. Engelkemier, M. Persico, P. Manikandan, and W. L. Hase, J. Phys. Chem. A **115**, 6603 (2011).

[114] M.V. Volkenstein, M.A. Elyashevich, and B.L. Stepanov, *Vibrations of Molecules Vol. 2* (State Publishers of Technical-Theoretical Literature, Moscow, 1949), in Russian.

[115] V. A. Sipachev, J. Mol. Struct (Theochem) **121**, 143(1985).

[116] C. F. Jackels, Z. Gu, and D. G. Truhlar, J. Chem. Phys. **102**, 3188 (1995), 3188 (1995).

[117] D. F. McIntosh, Theor. Chem. Acc. **125**, 177 (2010).

[118] J. von Neumann, J. Res. Nat. Bur. Stand., Appl. Math. Ser. **12**, 36 (1951).

[119] E. Wigner, Phys. Rev. **40**, 749 (1932).

[120] K. Husimi, Proc. Phys. Math. Soc. Jpn. **22**, 264 (1940).

[121] K. Takahashi, J. Phys. Soc. Jpn. **55**, 762 (1986).

[122] W. L. Hase, D. M. Ludlow, R. J. Wolf, and T. Schlick, J. Phys. Chem. **85**, 958 (1981).

[123] S. Grimme, Angew. Chem. Int. Ed. **52**, 6306 (2013).

[124] D. Sebastiani and M. Parrinello, J. Phys. Chem. A **105**, 1951 (2001).

[125] D. A. Wann, A. V. Zakharov, A. M. Reilly, P. D. McCaffrey, and D. W. H. Rankin, J. Phys. Chem. A **113**, 9511 (2009).

[126] M. Praprotnik and D. Janezi, J. Chem. Phys. **122**, 174103 (2005).

[127] M. Aida and M. Dupuis, J. Mol. Struct. (Theochem) **633**, 247 (2003).

[128] Dalton2013 : Dalton and LSDALTON http://www.daltonprogram.org/

[129] Dalton, a molecular electronic structure program, Release Dalton2013.X (2013), see http://daltonprogram.org.

[130] lsDalton, a linear scaling molecular electronic structure program, Release Dalton2013.X (2013), see http://daltonprogram.org.

[131] G. J. Martyna, M. E. Tuckerman, D. J. Tobias, and M. L. Klein, Mol. Phys. **87**, 1117 (1996).

[132] R. Lindh, A. Bernhardsson, G. Karlstrøm, and P-Å Malmqvist, Chem. Phys. Lett. **241**, 423 (1995).

[133] R. Fletcher, *Practical Methods of Optimization Vol.1—Unconstrained Optimization* (Wiley, New York, 1981).

[134] J. M. Bofill, J. Comput. Chem. **15**, 1 (1994).

[135] J. Baker, J. Comput. Chem. **14**, 1085 (1993).

[136] S. Reine, A. Krapp, M. F. Iozzi, V. Bakken, T. Helgaker, F. Pawlowski, and P. Salek, J. Chem. Phys. **133**, 044102 (2010).

[137] U. Ekström, Libtaylor software library `http://libtaylor.googlecode.com` **2009**.

[138] W. Humphrey, A. Dalke, and K. Schulten, J. Molec. Graphics. **14**, 33 (1996).

[139] K. Hansen, P. U. Andersson, and E. Uggerud, J. Chem. Phys. **131**, 124303 (2009).

[140] S. Grimme, J. Comput. Chem. **25**, 1463 (2004).

[141] N. Agmon, Chem. Phys. Lett. **244**, 456 (1995).

[142] H. S. Smalø and E. Uggerud, Mol. Phys. **111**, 1563 (2013).

[143] K. C. Neuman and A. Nagy, Nat. Meth. **5**, 491 (2008).

[144] T. J. Mason, Chem. Soc. Rev. **26**, 443 (1997).

I

II

III

IV

THE JOURNAL OF CHEMICAL PHYSICS **141**, 064108 (2014)

Sampling microcanonical ensembles of trajectories using harmonic approximation in internal coordinates

Vladimir V. Rybkin[1,a)] and Ulf Ekström[2]
[1]*G. A. Krestov Institute of Solution Chemistry of the Russian Academy of Sciences, Akademicheskaya St. 1, Ivanovo 153045, Russia*
[2]*Centre for Theoretical and Computational Chemistry, Department of Chemistry, University of Oslo, P.O. Box 1033, N-0315 Oslo, Norway*

(Received 16 June 2014; accepted 23 July 2014; published online 11 August 2014)

In this paper, we modify quasiclassical harmonic sampling of microcanonical ensembles of trajectories by using the curvilinear internal coordinates. The harmonic approximation in the curvilinear normal coordinates provides a more realistic description of the PES than in the conventional rectilinear ones at finite displacements. Therefore, the sampling of vibrations in the internal coordinates significantly improves the quality of the sampling in a block-box fashion, providing more realistic displacements and reducing the errors in the potential energy. In particular, the sampling of large-amplitude torsion vibrations, which is non-realistic in the Cartesian modes, becomes accurate or acceptable in the curvilinear modes. © *2014 AIP Publishing LLC*. [http://dx.doi.org/10.1063/1.4892109]

I. INTRODUCTION

Integrating microcanonical (NVE) ensembles of classical trajectories is an important and widely used tool to study the dynamics of gas-phase reactions. Most applications are performed by means of direct Born-Oppenheimer molecular dynamics with forces calculated on-the-fly by electronic structure theory methods.[1] A "swarm" of trajectories is usually integrated for the proper statistical averaging. Since NVE conditions require that the system is not interacting with the surroundings, no equilibration stage is present in the simulations. The results thus strongly depend on the initial conditions: coordinates and velocities. To generate realistic trajectories, one needs to have a good approximation to the initial state wave function or its classical analogue.[2] For adiabatic dynamics, a complete set of rotational-vibrational wave functions for the selected electronic state is required. However, accurate solution for the time-independent nuclear problem is computationally as demanding as trajectory simulations. Therefore, a simple "harmonic oscillator-rigid rotor" approximation is routinely used to obtain the starting conditions. In this paper, we restrict ourselves to sampling molecular vibrations.

The sampling procedure involves the following steps:[3–5]

- Find a stationary point $\mathbf{x}_0$ on the potential energy PES, calculate the molecular Hessian, $\mathbf{F}$.
- Solve the vibrational problem in the harmonic approximation.
- Sample quantum numbers (vibrational levels and, consequently, energies) according to the assumed energy distribution.
- Sample displacements and momenta (velocities) in normal coordinates.
- Transform displacements and velocities to the Cartesian frame, $\Delta\mathbf{x}$ and $\mathbf{v}$, calculate the harmonic potential, V^{harm}, and kinetic energies in the harmonic approximation.
- Calculate the Born-Oppenheimer potential energy $\mathbf{x}_0 + \Delta\mathbf{x}$, V, by electronic structure theory.
- Scale $\Delta\mathbf{x}$ and so that $V^{\text{harm}} = V$.

The first two steps are performed once, whereas the others are repeated for each trajectory in the set. The scaling in the final step is meant to introduce the corrections for anharmonicity which inevitably comes out for finite displacements from the stationary point. Although this procedure gives the correct energy (macrostate), it distorts the microstate since coordinates are scaled uniformly although their contributions to anharmonicity are different.

It is thus desirable to reduce sampling errors without going beyond the harmonic approximation. In this paper, we are going to show that it is possible by solving the harmonic vibrational problem in curvilinear internal coordinates—bond lengths, valence, and torsion angles, etc. Being chemically natural they are known to result in smaller couplings and anharmonicities than the Cartesian coordinates do.

II. THEORY

A. Curvilinear internal coordinates

First, we define the system of internal coordinates $\mathbf{q}(\mathbf{x})$ which are explicit functions of the Cartesian coordinates $\mathbf{x}$. In general case, $\mathbf{q}$ may be a redundant set. The Jacobian used for transformation between the two systems is known as the $\mathbf{B}$-matrix: $B_{ij} = \frac{\partial q_i}{\partial x_j}$.[6] If $\mathbf{q}$ are redundant then the problem should be solved using a non-redundant set $\mathbf{s}$, which spans the range of $\mathbf{B}$ and is defined by some linear transformation:

$$\mathbf{s} = \mathbf{U}^t\mathbf{q}. \tag{1}$$

a)Electronic mail: rybkinjr@gmail.com. Also at Centre for Theoretical and Computational Chemistry, Department of Chemistry, University of Oslo, P.O. Box 1033, N-0315 Oslo, Norway.

In this work, we use the redundant set of primitive internal coordinates[7,8]—bond lengths, valence, and torsion angles – **q** – and the non-redundant coordinates – **s** – are delocalized internal coordinates.[9] They are found by singular value decomposition of **B** and **U** is composed of non-redundant right-singular vectors. The Jacobian between **x** and **s** is now

$$\mathbf{B_s} = \mathbf{U}^t\mathbf{B}. \tag{2}$$

B. Harmonic vibrations in internal coordinates

To sample the trajectories, we need to solve the vibrational harmonic problem in internal coordinates. These have been accomplished in several publications, namely, in Refs. 10–13 and a more accurate approach by Sipachev.[14] Here we the use formulation of Jensen and Palmer,[13] according to which the harmonic vibrational problem in curvilinear internal coordinates is solved by the following secular equation:

$$\left(\mathbf{G_m}^{1/2}\mathbf{F_s}\mathbf{G_m}^{1/2}\right)\mathbf{V} = \mathbf{V}\mathbf{\Lambda}. \tag{3}$$

In this equation, $\mathbf{F_s}$ is the force constant matrix (molecular Hessian) in delocalized internal coordinates, which is for the special case of PES extremum defined as follows:

$$\mathbf{F_s} = \left(\mathbf{B_s}^t\right)^+\mathbf{F}\mathbf{B_s}^+, \tag{4}$$

and $\mathbf{G_m}$ is the kinetic energy matrix:

$$\mathbf{G_m} = \mathbf{B_s}\mathbf{M}^{-1}\mathbf{B_s}^t, \tag{5}$$

where **M** is a diagonal matrix of nuclear masses. Here, + denotes the Moore-Penrose pseudoinverse. Note that, unlike for the harmonic problem in Cartesian coordinates, the kinetic operator $\mathbf{G_m}$ is not exact since nonlinear terms arising upon coordinate transformation are truncated.

Vibrational frequencies are defined by the eigenvalues $\mathbf{\Lambda}$ and curvilinear normal coordinates **L** are found as

$$\mathbf{L} = \mathbf{G_m}^{1/2}\mathbf{V}. \tag{6}$$

C. Sampling

As soon as vibrational frequencies and normal coordinates are found, sampling is performed. Quantum numbers are selected manually or found by a procedure such as the von Neumann rejection technique.[15] Once that has been done, displacements and velocities may be sampled either in a classical[3,4] or in a quantum[4] manner using Wigner[16] or else Husimi[17,18] functions.

In this paper, we sample the Boltzmann distribution for each of the modes at a certain temperature and find canonical coordinates and momenta for the *i*th mode classically as follows:

$$Q_i = (2E_i/f_i)^{1/2}\cos 2\pi R_i, \tag{7}$$

$$P_i = (2E_i)^{1/2}\sin 2\pi R_i, \tag{8}$$

where E_i is the energy of the harmonic vibration in the selected state, f_i is the corresponding vibrational eigenvalue, and R_i is a newly generated random number uniformly distributed on [0, 1]. The classical vibrational amplitude is

$$A_i = (2E_i/f_i)^{1/2}. \tag{9}$$

D. Internal to Cartesian-back transformation

Once displacements are defined, they need to be transformed to the Cartesian frame, since Cartesian coordinates are required to calculate electronic energy. Displacements in non-redundant internal coordinates are obtained trivially:

$$\Delta\mathbf{s}(\mathbf{Q}) = \mathbf{L}\mathbf{Q}. \tag{10}$$

To find Cartesian displacements $\Delta\mathbf{x}(\mathbf{Q})$ corresponding to $\Delta\mathbf{s}(\mathbf{Q})$ is more difficult, since the latter are nonlinear functions of the former. Nevertheless, internal to Cartesian back-transformation can be performed up to a given accuracy by several methods: iterative back-transformation,[19] simplified iterative back-transformation,[20,21] transformation using auxiliary Z-matrix,[20] and the method using reciprocal vector bases.[10] Here we apply the recently developed high-order path expansion (HOPE) back-transformation,[22] using high-order geometric derivatives of the internal coordinates with respect to the Cartesian ones, computed by automatic differentiation techniques.

E. Scaling

If $V^{\text{harm}}(\Delta\mathbf{x})$ and $V(\Delta\mathbf{x})$ are the potential energy in the harmonic approximation, and the true Born-Oppenheimer potential energy at finite displacement $\Delta\mathbf{x}$, respectively, then the following scaling:

$$\mathbf{x}' = k^{1/2}\mathbf{x}, \tag{11}$$

$$k = \frac{V^{\text{harm}}(\Delta\mathbf{x})}{V(\Delta\mathbf{x})}, \tag{12}$$

leads to $V^{\text{harm}}(\Delta\mathbf{x}') = V(\Delta\mathbf{x})$. Velocities are scaled accordingly to preserve the equality of the potential and kinetic energies in the harmonic approximation:

$$\mathbf{v}' = k^{-1/2}\mathbf{v}. \tag{13}$$

Such scaling assumes that k is close to 1 and is meant to make starting conditions more realistic.

Here we introduce two scaling coefficients depending on how the finite displacement has been generated: using rectilinear normal modes, k_x, or curvilinear ones, k_s.

III. COMPUTATIONAL CONSIDERATIONS

From computational point of view, the most expensive procedure in this scheme is the internal-to-Cartesian back transformation,[22] which is to be performed once for each trajectory. The cost of the transformation itself is dominated by the cost of inverting the Wilson's **B** matrix. Thus, the use of the HOPE[22] transformation, requiring only one inversion for $\mathbf{B}(\mathbf{x}_0)$ for all M trajectories in the ensemble, will not add any significant computational time to the procedure. By contrast, conventional iterative back-transformation[19] requires on

average 5–10 matrix inverses to transform $\Delta \mathbf{s}_i$ into $\Delta \mathbf{x}_i$, that is, from $5M$ to $10M$ inversions are to be computed for each member of the whole ensemble. Consequently, sampling may take non-negligible time compared to electronic structure calculations, especially for big M. Indeed, integrating hundreds of trajectories is not uncommon in applications (see Ref. 1).

IV. RESULTS AND DISCUSSION

We test our algorithm on the acetone molecule CH_3–CO–CH_3 in its equilibrium geometry where the force constant matrix has been calculated and the harmonic vibrational problem has been solved. First, to probe the difference between curvilinear and rectilinear normal coordinates we perform energy scans along the normal modes. After that, we go on to sample the ensembles of trajectories at various temperatures.

All electronic structure calculations have been performed using DALTON[24,26] and LSDALTON[25,26] programs at DFT/BLYP[27,28]/6-311G**[29] level of theory and the sampling has been made with a Python script. To perform HOPE back-transformation automatic differentiation library libtaylor[23] has been applied.

A. PES scans

Solving the harmonic problem for acetone in Cartesian and internal coordinates results in vibrational frequencies identical within fractions of cm^{-1}. In Figs. 1 and 2 we have plotted energy scans along the three lowest-frequency modes at the given level of electronic structure theory: $\nu_1 = 23\ cm^{-1}$ corresponding to conrotatory torsion of methyl groups, $\nu_2 = 133\ cm^{-1}$ corresponding to disrotatory torsion of methyl groups, and $\nu_3 = 368\ cm^{-1}$ which is the deformation of carbon skeleton of the molecule. The range of displacement is extended up to two classical ground-state amplitudes A_i, as the regions of space beyond A_i are accessible for excited states in case of classical sampling and for any state in case of quantum-mechanical sampling. From Figs. 1 and 2 it becomes immediately apparent that harmonic approximation in curvilinear internal coordinates is a much better one than in Cartesian. In case of both, torsional vibrations for finite displacements from the equilibrium, the latter fails almost immediately.

For ν_1, although k_s drops to the value of 0.1 and more, it is everywhere about two orders of magnitude smaller than k_x. For ν_2 in the range under consideration there is essentially no anharmonicity in curvilinear coordinates and k_s is everywhere close to one. Unlike this, rectilinear harmonic approximation

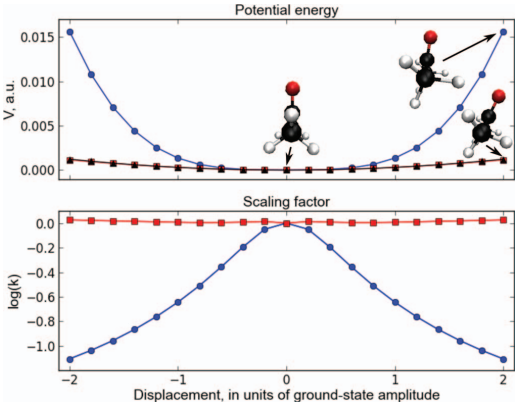

FIG. 2. Torsional vibration ν_2: PES scan with illustrations of geometric displacements (top) and scaling coefficients (bottom). Black—harmonic potential; blue—scan in rectilinear normal coordinates and k_x; and red—scan in curvilinear normal coordinates and k_s.

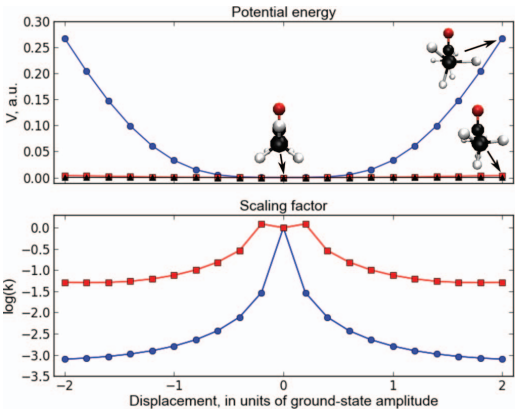

FIG. 1. Torsional vibration ν_1: PES scan with illustrations of geometric displacements (top) and scaling coefficients (bottom). Black—harmonic potential; blue—scan in rectilinear normal coordinates and k_x; and red—scan in curvilinear normal coordinates and k_s.

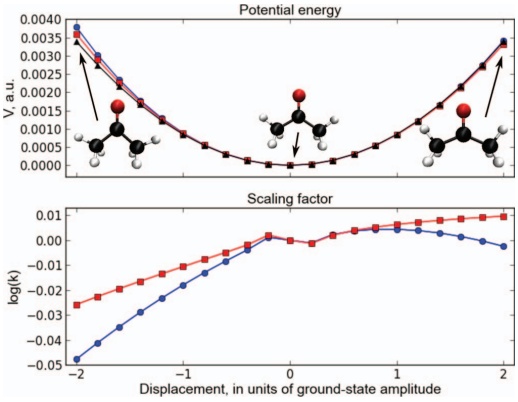

FIG. 3. Deformational vibration ν_3: PES scan with illustration of geometric displacements (top) and scaling coefficients (bottom). Black—harmonic potential; blue—scan in rectilinear normal coordinates and k_x; and red—scan in curvilinear normal coordinates and k_s. The difference between Cartesian and internal coordinate step geometries is visually indistinguishable on the scale of the figure, and only the Cartesian step geometry is shown.

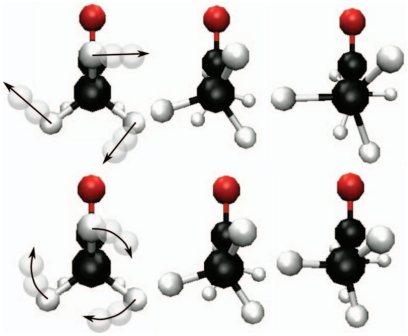

FIG. 4. Illustration of the difference between normal mode following in Cartesian coordinates (top), and internal coordinates (bottom) for the lowest torsional mode of acetone (motion shown in one direction only).

again fails to represent the true section of the PES. Therefore, by using curvilinear internal coordinates, the harmonic approximation is significantly improved in the case of ν_1 and becomes qualitatively accurate in case of ν_2 as compared to conventional rectilinear normal coordinates.

For the deformation ν_3 (see Fig. 3) both harmonic curves follow the true PES quite closely, with the curvilinear normal mode scan being slightly more accurate for folding the C–C–C skeleton and the rectilinear normal mode scan being better for unfolding. Nevertheless, on average the curvilinear description is slightly preferable. Other vibrations with higher frequencies do not exhibit any noticeable differences between the representations.

The reason for the complete failure of the harmonic approximation in the Cartesian coordinates in case of ν_1 and ν_2 is the rapid increase of the coupling between them and the C–H bonds stretching at finite displacements. If internal coordinates are used, the contribution of this coupling is also significant for the lower-frequency torsion, but is already negligible for the higher-frequency vibration. These statements are illustrated in Fig. 4. It is clearly seen that for ν_1 C–H bonds are significantly stretched in case of rectilinear-mode scan. In fact, at $2A_1$ they are elongated ca. 50% with respect to the equilibrium length. The analogous elongation for ν_2 is about 25%. In case of the curvilinear normal modes, C–H elongation is much smaller for ν_1 and insignificant for ν_2. Such dramatic effects of coordinate system choice become apparent for large-amplitude vibrations involving angular coordinates, that is, low-frequency ones such as methyl group torsions.

B. Sampling trajectories

After having ensured that the use of curvilinear internal coordinates indeed improves the harmonic description of large-amplitude vibrations in acetone, we have sampled three sets of 300 trajectories each from the Boltzmann distribution at three temperatures: 300 K, 500 K, and 700 K. To facilitate the comparison, we used the same vibrational quantum numbers and random phases in Eq. (7) for both curvilinear and rectilinear-mode sampling. The results are given in Table I.

It is readily seen from these data that using curvilinear normal coordinates reduces both accumulated and maximal error in potential energy substantially. RMS deviation of scaling coefficient is also reduced by about a factor of two. Average values of k are less representative as measures of error, since k can be both greater and smaller than 1.0, leading to error cancellation after averaging. Nevertheless, average values of the scaling factors are instructive: the fact that they are in all cases smaller than 1.0, especially for the rectilinear modes, points at the dominant source of errors—sampling of torsional vibrations. Indeed, as we have seen from Figures 1 and 2, the harmonic approximation underestimates the potential energy, and the maximal errors for the sampling in the rectilinear normal coordinates correlate quite well with those for the PES scans at large displacements (especially for ν_1).

Much, or even most, energy is contained in the higher-frequency modes, which are generally well described by the harmonic approximation. Unreasonable displacements along the low-frequency modes involving angular coordinates lead to significant errors, often compatible with the energy of high-frequency vibrations. As a result, the scaling factor deviates from 1.0 significantly but reflects neither the accuracy of sampling high-frequency modes, nor low-frequency modes. For the former, it is too far from 1.0, for the latter—too close to it. Consequently, by global scaling (Eq. (11)) it is impossible to fix unphysical displacements arising from large-amplitude vibrations. Moreover, this procedure will automatically spoil the quality of the low-amplitude vibrations sampling. Fortunately, this problem can be reduced, and in some cases solved completely, by performing the harmonic sampling in the curvilinear internal coordinates. A possible extension of the scheme can be designed based on the idea of mode-specific scaling, which goes beyond the scope of present work.

C. Trajectory modelling results

Finally, we have integrated two sets of 100 trajectories for acetone sampled at 300 K in the Cartesian and in the internal coordinates. The gradient-based velocity-Verlet integrator[30]

TABLE I. Sampling of acetone at 300, 500, and 700 K using rectilinear and curvilinear normal coordinates at DFT/BLYP/6-311G** level of theory.

	Mean error (a.u.)		Maximal error (a.u.)		Mean deviation of k from 1.0		Average k	
	Rect.	Curv.	Rect.	Curv.	Rect.	Curv.	Rect.	Curv.
300 K	0.032	0.013	0.220	0.053	0.245	0.135	0.774	0.920
500 K	0.032	0.013	0.168	0.036	0.241	0.126	0.789	0.939
700 K	0.035	0.013	0.410	0.052	0.248	0.130	0.777	0.927

with the time step of 0.5 fs was applied, and the guess density was propagated using the time-reversible technique.[31] The trajectories were run up to 5000 steps, or 2.5 ps.

In turned out that 45% of trajectories initialized using rectilinear modes resulted in the dissociation of one or several C–H bonds within 20 fs. On the contrary, only 5% of trajectories ended up in C–H bond breaking, when curvilinear normal modes were used for the sampling. This unphysical behaviour is the consequence of the coupling between the stretch and the torsion, especially strong in the case of Cartesian modes, as discussed above and plotted in Figs. 1 and 2. Typically, such problems are coped with by sampling several modes according to the classical velocity-distribution. However, this can be largely avoided by sampling in the internal coordinates.

V. CONCLUSIONS

We have shown that sampling low-frequency (large-amplitude) vibrations (especially those involving angular coordinates) using the conventional rectilinear normal coordinates is, even for small displacements, a very inaccurate procedure which cannot be improved by global coordinate scaling. The reason is that the scaling factor is defined to a large extent by high-frequency modes, which are well described by the (Cartesian) harmonic approximation, whereas the errors originate from low-frequency vibrations. On the other hand, using the curvilinear normal modes significantly improves the quality of the sampling in a simple black-box fashion, which requires almost no additional computational effort provided the HOPE internal-to-Cartesian back transformation is used.

An important application of the present approach would be sampling of rotational modes of individual molecules in molecular clusters. In this case, it may, however, be necessary to introduce new types of redundant internal coordinates, exactly as suggested in Ref. 13. Here, the new internal coordinates should correspond to the rotation of entire molecules. Because of this additional complication we leave molecular clusters as a topic for future work.

ACKNOWLEDGMENTS

This work was supported by the Norwegian Research Council through the CoE Centre for Theoretical and Computational Chemistry (CTCC) Grant Nos. 179568/V30 and 171185/V30 and through the European Research Council under the European Union Seventh Framework Program through the Advanced Grant ABACUS, ERC Grant Agreement No. 267683.

[1] M. Paranjothy, R. Sun, Y. Zhang, and W. L. Hase, WIREs: Comput. Mol. Sci. **3**, 296–316 (2013).
[2] P. Manikandan and W. L. Hase, J. Chem. Phys. **136**, 184110 (2012).
[3] W. L. Hase and D. G. Buckowski, Chem. Phys. Lett. **74**, 284 (1980).
[4] K. Park, J. Engelkemier, M. Persico, P. Manikandan, and W. L. Hase, J. Phys. Chem. A **115**, 6603 (2011).
[5] W. L. Hase, D. M. Ludlow, R. J. Wolf, and T. Schlick, J. Phys. Chem. **85**, 958 (1981).
[6] E. B. Wilson, J. C. Decius, and P. C. Cross, *Molecular Vibrations* (McGraw-Hill, New York, 1955).
[7] P. Pulay and G. Fogarasi, J. Chem. Phys. **96**, 2856 (1992).
[8] C. Y. Peng, P. Y. Ayala, H. B. Schlegel, and M. J. Frisch, J. Comput. Chem. **17**, 49 (1996).
[9] J. Baker, A. Kessi, and B. Delley, J. Chem. Phys. **105**, 192 (1996).
[10] H. Dachsel, D. Sosna, and W. Quapp, J. Mol. Struct: THEOCHEM **315**, 315 (1994).
[11] C. F. Jackels, Z. Gu, and D. G. Truhlar, J. Chem. Phys. **102**, 3188 (1995).
[12] D. F. McIntosh, Theor. Chem. Acc. **125**, 177 (2010).
[13] F. Jensen and D. S. Palmer, J. Chem. Theory Comput. **7**, 223 (2011).
[14] V. A. Sipachev, J. Mol. Struct: THEOCHEM **121**, 143 (1985).
[15] J. von Neumann, Various techniques used in connection with random digits, J. Res. Nat. Bur. Stand., Appl. Math. Ser. **12**, 36–38 (1951) [reprinted in Collected Works, Vol. 5 (Pergamon, 1963), pp. 768–770].
[16] E. Wigner, Phys. Rev. **40**, 749 (1932).
[17] K. Husimi, Proc. Phys. Math. Soc. Jpn. **22**, 264 (1940).
[18] K. Takahashi, J. Phys. Soc. Jpn. **55**, 762 (1986).
[19] P. Pulay, G. Fogarasi, F. Pang, and J. E. Boggs, J. Am. Chem. Soc. **101**, 2550 (1979).
[20] J. Baker, D. Kinghorn, and P. Pulay, J. Chem. Phys. **110**, 4986 (1999).
[21] V. Bakken and T. Helgaker, J. Chem. Phys. **117**, 9160 (2002).
[22] V. V. Rybkin, U. Ekström, and T. Helgaker, J. Comput. Chem. **34**, 1842 (2013).
[23] U. Ekström, Libtaylor Software Library, 2009, see http://libtaylor.googlecode.com (accessed May 14, 2013).
[24] Dalton, a molecular electronic structure program, Release DALTON2013.0, 2013, see http://daltonprogram.org.
[25] LSDALTON, a linear scaling molecular electronic structure program, Release Dalton2013, 2013, see http://daltonprogram.org/.
[26] K. Aidas, C. Angeli, K. L. Bak, V. Bakken, R. Bast, L. Boman, O. Christiansen, R. Cimiraglia, S. Coriani, P. Dahle, E. K. Dalskov, U. Ekström, T. Enevoldsen, J. J. Eriksen, P. Ettenhuber, B. Fernandez, L. Ferrighi, H. Fliegl, L. Frediani, K. Hald, A. Halkier, C. Hättig, H. Heiberg, T. Helgaker, A. C. Hennum, H. Hettema, E. Hjertenæs, S. Høst, I.-M. Høyvik, M. F. Iozzi, B. Jansik, H. J. Aa. Jensen, D. Jonsson, P. Jørgensen, J. Kauczor, S. Kirpekar, T. Kjærgaard, W. Klopper, S. Knecht, R. Kobayashi, H. Koch, J. Kongsted, A. Krapp, K. Kristensen, A. Ligabue, O. B. Lutnæs, J. I. Melo, K. V. Mikkelsen, R. H. Myhre, C. Neiss, C. B. Nielsen, P. Norman, J. Olsen, J. M. H. Olsen, A. Osted, M. J. Packer, F. Pawlowski, T. B. Pedersen, P. F. Provasi, S. Reine, Z. Rinkevicius, T. A. Ruden, K. Ruud, V. Rybkin, P. Salek, C. C. M. Samson, A. Sanchez de Meras, T. Saue, S. P. A. Sauer, B. Schimmelpfennig, K. Sneskov, A. H. Steindal, K. O. Sylvester-Hvid, P. R. Taylor, A. M. Teale, E. I. Tellgren, D. P. Tew, A. J. Thorvaldsen, L. Thøgersen, O. Vahtras, M. A. Watson, D. J. D. Wilson, M. Ziolkowski, and H. Ågren, "The Dalton quantum chemistry program system," WIREs: Comput. Mol. Sci. **4**, 269 (2014).
[27] A. D. Becke, Phys. Rev. A **38**, 3098 (1988).
[28] C. Lee, W. Yang, and R. G. Parr, Phys. Rev. B **37**, 785 (1988).
[29] R. Krishnan, J. S. Binkley, R. Seeger, and J. A. Pople, J. Chem. Phys. **72**, 650 (1980).
[30] L. Verlet, Phys. Rev. **159**, 98 (1967).
[31] A. M. N. Niklasson, C. J. Tymczak, and M. Challacombe, Phys. Rev. Lett. **97**, 123001 (2006).